

AMERICAN UNIVERSITY OF BEIRUT

EVAPORATION KINETICS OF SECONDARY
ORGANIC AEROSOL FORMED FROM
GASOLINE ENGINE EMISSIONS

by

MARIAM MOHAMAD FAWAZ

A thesis

submitted in partial fulfillment of the requirements
for the degree of Master of Engineering
to the Department of Mechanical Engineering
of the Faculty of Engineering and Architecture
at the American University of Beirut

Beirut, Lebanon
March 2015

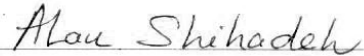
AMERICAN UNIVERSITY OF BEIRUT

EVAPORATION KINETICS OF SECONDARY
ORGANIC AEROSOL FORMED FROM
GASOLINE ENGINE EMISSIONS

by

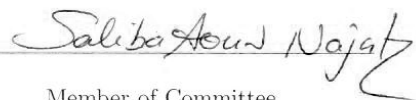
MARIAM MOHAMAD FAWAZ

Approved by:



Dr. Alan Shihadeh, Professor
Mechanical Engineering

Advisor



Dr. Najat Saliba, Professor
Chemistry

Member of Committee



Dr. Issam Lakkis, Associate Professor
Mechanical Engineering

Member of Committee

Date of thesis defense: March 26, 2015

AMERICAN UNIVERSITY OF BEIRUT

THESIS, DISSERTATION, PROJECT
RELEASE FORM

Student Name: fawaz Mariam Mohamad
Last First Middle

Master's Thesis Master's Project Doctoral Dissertation

I authorize the American University of Beirut to: (a) reproduce hard or electronic copies of my thesis, dissertation, or project; (b) include such copies in the archives and digital repositories of the University; and (c) make freely available such copies to third parties for research or educational purposes.

I authorize the American University of Beirut, **three years after the date of submitting my thesis, dissertation, or project**, to: (a) reproduce hard or electronic copies of it; (b) include such copies in the archives and digital repositories of the University; and (c) make freely available such copies to third parties for research or educational purposes.

Mfawaz April 30, 2015
Signature Date

Acknowledgements

I thank God for giving me blessings beyond my count and more than I deserve.

I would like to express my deep gratitude to my adviser Dr. Alan Shihadeh. I have been truly fortunate to work under his supervision in the Aerosol Lab.

I am grateful for Dr. Najat Saliba and Dr. Issam Lakkis for serving on my thesis committee.

I am thankful and blessed to have my two older brothers, the dudes, Kassem and Ahmad for guiding me every step of the way and being the harshest critics while always treating me as their little sister. Also I thank my father for being there, driving me around no matter how late at night and always being interested in my work. I am Ever After indebted to my mother who bore the responsibility of supporting me throughout the toughest of situations. Most importantly, for teaching me that being a female is never an excuse.

An Abstract of the Thesis of

Mariam Mohamad Fawaz for Master of Engineering
Major: Mechanical Engineering

Title: Evaporation Kinetics of Secondary Organic Aerosols

The discrepancy between measured and modeled concentrations of secondary organic aerosols (SOA) in the atmosphere is triggering studies to challenge the adopted theories of partitioning between the gas and the condensed phase of aerosols. Absorptive partitioning theory, a traditionally adopted model for SOA concentration estimation, predicts rapid reversible partitioning of particles in the atmosphere due to evaporation; however reports have been emerging on the limitations of the applicability of this theory, citing low evaporation coefficients due to the amorphous state of SOA. In our approach we studied the evaporation kinetics of SOA produced from the photochemical oxidation of gasoline engine emissions. We evaluated the equilibration time and calculated the evaporation coefficient using thermodynamic data calculated in our experiments rather than using previously published data. SOA particles were produced in a flow reactor and isothermally diluted in a smog chamber; the particles were allowed to evaporate for a period of time starting at atmospherically relevant concentrations. In the evaporation model, we used mass transfer equations to describe diffusion of molecules between the surface and the interface at the transition flow regime using the Fuch-Sutugin factor. We also accounted for losses due to particle deposition on the walls of the smog chamber. To fit the recorded results from the chamber experiment, we represented the size distribution of SOA using the concept of the condensation sink diameter. Based on the experiment results we were able to observe equilibrium nearly after an hour, and calculated an average value of the evaporation coefficient of 0.06. We can report that SOA from anthropogenic sources did not exhibit hindered evaporation rates and reached equilibrium within the timescales of the experiment.

Contents

Acknowledgements	vii
Abstract	viii
1 Introduction	1
1.1 SOA Absorptive Partitioning Theory	2
1.2 Limitations of Absorptive Partitioning	3
1.3 Previous Work	5
1.4 Objective	8
2 Theory	9
2.1 Evaporation of an Unbounded Aerosol	9
2.2 Particle Evaporation in an Enclosure	14
2.3 Equilibrium Approach	17
3 Materials and Methods	20
3.1 Experimental Setup	20
3.2 Experimental Procedure	22
3.3 Experimental Conditions	24
3.4 Methods	25
3.5 Code Description	29
4 Results	35
5 Discussion	41
5.1 SOA Volatility	41
5.2 Evaporation Coefficient	44
6 Conclusion	48
A Abbreviations	50

List of Figures

2.1	The evaporation of a stagnant particle in a surrounding gas. C_g is the gas phase concentration away from the particle, C_{sat} is the vapor saturation ratio, and r is the radius of the particle.	10
2.2	The interactions of the molecules occurring at the interface of a particle, molecules may collide with other molecules or released immediately to the surrounding gas.	13
2.3	Particle interaction in the smog chamber. The considered interactions are deposition of the particles on the chamber walls, the evaporation of particles to reach equilibrium and the evaporation of deposited particles on the walls	14
2.4	Change in saturation ratio throughout the experiment, from PAM to the smog chamber	18
3.1	Process flow diagram. The PAM is the potential aerosol mass reactor, the CPC is the condensation particle counter, the DMA is the differential mobility analyzer and E is the gasoline engine	21
3.2	Typical particle size distribution of SOA in the chamber after isothermal dilution for (a) Number distribution (b) Volume distribution	26
3.3	The simulated trend of change of the condensation sink diameter governed by particle loss and evaporation separately	28
3.4	The typical result of a corrected condensation sink diameter and the uncorrected condensation sink diameter.	29
3.5	Evaporation model code algorithm	34
4.1	The equilibration profile of the condensation sink diameter measured over time for the four experiments (a) experiment A, (b) experiment B, (c) experiment C, (d) experiment D	36
4.2	The rise in the saturation ratio during evaporation simulated at different evaporation coefficient values, and the result calculated from experiment C	38
4.3	The variation of the individual evaporation coefficient of each experiment at selected ω values	39

4.4	The variation of the evaporation coefficient as a function of molecular weights modelled using the results of experiment C.	40
4.5	The variation of the evaporation coefficient as a function of gas diffusion coefficient modelled using the results of experiment C. . .	40
5.1	Saturation concentrations of organic aerosols cited in literature at 298K, ARL are the results from our experiments, LV-OOA is low volatility oxygenated organic aerosol, OOA is oxygenated organic aerosol, HV-OOA is high volatility oxygenated aerosol, OA is organic aerosol, SOA ₁ produced from pentadecane, and SOA ₂ from α -pinene.	43
5.2	Model fit results of SOA particle evaporation before approaching equilibrium according to different values of saturation concentrations.	46

List of Tables

3.1	The initial conditions of the four SOA evaporation experiments .	25
3.2	The initial conditions of the four SOA evaporation experiments .	25
3.3	Physical Parameters used in the evaporation model for the base case calculations	32
4.1	The calculated results of the evaporation coefficient, the saturation concentration and equilibration time from the evaporation model .	37
5.1	Saturation Concentrations of SOA calculated from the four experiments at 298K	42

Chapter 1

Introduction

Air pollution, represented by an increasing concentration of fine particulates in the atmosphere, is highly related to an increasing mortality rate, mainly due to cardiopulmonary diseases [1]. Fine particulate matter in the atmosphere are the particles that have a diameter of $2.5\mu\text{m}$ or smaller denoted by $\text{PM}_{2.5}$; these could be emitted directly to the atmosphere or formed from gas precursors in reactions in the atmosphere [2]. Organic aerosols belonging to $\text{PM}_{2.5}$ constitute 30%-80% of the particles in the troposphere [3]. Owing to their hydrophilic nature, organic aerosol present in the upper troposphere act as cloud condensation nuclei [4]. These organic aerosols fall into two subcategories: (1) particles that are formed from the condensation of gas phase oxidation products to the particle phase referred to as secondary organic aerosols (SOA) (2) are the vapors that condense to particle phase in the atmosphere referred to as primary organic aerosols (POA) [5].

Transport and formation models [5, 6, 7, 8, 9] attempt to predict the concentration of organic aerosols in the atmosphere. The model results are then used for predicting the effect of organic aerosol concentrations on the climate

and human health. This necessitates a full knowledge of the dynamics of particle condensation and evaporation during formation and throughout the life of the particle in the troposphere.

Traditional models predict SOA concentrations according to the equilibrium partitioning between the condensed phase coexisting with its gas phase. These have assumed rapid reversible equilibrium partitioning from the gas phase to the condensed phase and from the condensed phase to the gas phase; partitioning is then driven by the concentration gradient. The models account for thermodynamics and mass transfer resistance at the interface between the particle surface and the gas surrounding it. Despite the numerous studies, SOA partitioning is still poorly understood and underpredicted.

1.1 SOA Absorptive Partitioning Theory

The partitioning models study the condensation of gas phase oxidation products onto existing particles to understand the formation and growth of SOA; the model also studies the reversibility of the partitioning by examining the evaporation of particles at a perturbed state. Absorptive equilibrium partitioning introduced by Pankow [10, 11] is a widely used method for modeling SOA partitioning in the atmosphere [12, 13, 14, 15, 16, 17, 18]. In this model, SOA particle growth occurs when gas phase oxidation products condense onto existing seeds by absorption such as ammonium sulfate [19]. Growth was thought to advance until the concentration of the surrounding gas decreases, by condensation into particle, to reach the saturation concentration of the particle hence the system of the particle and gas reaches equilibrium [20]. However, absorptive partitioning theory extended the growth of the particle at

gas concentrations below the saturation concentration. The basic assumption to the applicability of the absorptive partitioning theory is that the particles are well-mixed sub-cooled particles.

Later work by Odum *et al.* [21] applied the absorptive partitioning theory to model SOA formation. SOA formation was represented by the formation of two products, a semivolatile and a nonvolatile product, to act as a surrogate of the tens of products formed from the oxidation of the reactive organic gas. Since the two-product model was able to fit the previous experimental work reported in literature on the yield of SOA [22], the parametrization of SOA product formation was further developed to include four and seven surrogate products with different saturation pressures ranging from non-volatile, semi-volatile, and to intermediate-volatile product [23, 24, 18, 25]. These studies distinguish between products of SOA according to the conditions of formation including the parent reactive gas, irradiation exposure, temperature, and relative humidity. The division of condensed phase products according to their volatilities then led way to the introduction of the volatility basis set of SOA [26, 27, 28] that predicts the division of products according to their saturation concentrations after aging, dilution, cooling and heating.

1.2 Limitations of Absorptive Partitioning

Amid the wide acceptance of the absorptive partitioning theory, recent evaporation experiments [29, 30, 31] have been reported not to follow rapid reversible partitioning as dictated by the absorptive partitioning theory. They also claim that the traditionally considered near unity evaporation coefficient of SOA particles, is unrealistic [29, 30, 32]. They attribute the reasons of this

departure from the theory to evidence that SOA particles are not well represented by the assumptions of being well-mixed and subcooled. Instead, particles exist in an amorphous solid state with low rates of intra-particle mass transfer [33, 34, 35] or that particles are viscous due to the formation of low volatility oligomers in the particle, making bulk diffusion the rate limiting step rather than surface mass transfer. Thus, particles responding to changes in the atmosphere require long times to reach equilibrium.

Oligomerization in particles have been reported to occur after formation at different timescales [36, 37, 38, 39] Perraud *et al.* [40] observed the formation of oligomers in α -pinene oxidized SOA due to the impinging vapors reacting at the surface. Under enough residence time, oligomers and unreacted vapors are then buried in the bulk of the particle. Particles formed are low volatility viscous particles that do not represent particles studied in the absorptive partitioning theory, and thus the partitioning theory does not hold.

The second challenge was the mixing state of SOA, different approaches have attempted to model and evaluate the mixing behavior between different components leading to the formation of SOA particles. The premise was that particle mixing reflects the rates of evaporation and the ability to use the absorptive partitioning theory. Determining the state of mixing of the particle provides a clue on whether intrinsic kinetic limitations or thermodynamic limitations govern the particle evaporation rate and thus the applicability of the absorptive partitioning theory. Hildebrandt *et al.* [41] evaluated the mixing of α -pinene seeded toluene oxidation products and toluene seeded α -pinene oxidation products. They tested the yields of toluene and α -pinene experiments according to aerosol mass yield results; the data of toluene and α -pinene oxidized SOA was found to be consistent with pseudoideal mixing, confirming the

assumption of the absorptive partitioning theory. Robinson *et al.* [42] produced SOA from α -pinene and toluene; toluene was seeded on α -pinene where both were produced separately. Significant mass from the toluene was mixed into the α -pinene SOA seed. In contrast to these findings [41, 42], the results of α -pinene oxidized SOA coated toluene oxidized SOA particles showed that the mixing of a particle cannot be determined simply by a well-mixed, pseudoideal, or core and shell. Instead particle composition according to the reacting species and atmospheric conditions dictate the degree of mixing and evaporation of the particle [43].

The third challenged assumption in the absorptive partitioning theory is that SOA exists in an amorphous solid state rather than a liquid-like state in the atmosphere. The crystalline state of SOA particles depends on their hygroscopic characteristics and the formation temperatures in the atmosphere [35]. Hence, adapting the absorptive partitioning model to the physical state of SOA, by using a correct vapor pressure corresponding to the specific particles being studied, will match the observed long equilibration times with the results of the model.

1.3 Previous Work

Laboratory chambers, usually referred to as smog chambers, are Teflon-made flexible bags that vary in size (3m^3 - 90m^3), used for the close study of physical and chemical interactions of particles. The advantage of using chambers for studying evaporation of particles is that they provide long experimental timescales and allow performing experiments at atmospherically relevant concentrations. Chamber studies are utilized to report the behavior of SOA

upon the introduction of a temperature or concentration step change. Temperature step changes are a sudden temperature change or a ramp in temperature through the experiment while concentration step changes are performed by diluting the smog chamber to cause a sudden decrease in particle concentration. In the following, we discuss the main findings.

Grieshop *et al.* [44] studied the reversibility of gas particle partitioning by isothermal dilution of fresh produced SOA from α -pinene in a 10m³ teflon chamber. During the experiment, 60% of that mass were lost during dilution. Then 40% of the remaining mass was lost in 2.5 hours during evaporation of the SOA particles till it reached equilibrium. According to the equilibrium time, the evaporation coefficient (defined in Chapter 2) was suggested to lie in the range of [0.01 0.001]. They compared the partitioning of SOA between the particle and gas phase at equilibrium with traditional SOA yield data of partitioning between phases after formation, and found the data to be in agreement thus showing that the partitioning of SOA is reversible. However, they attributed slow evaporation rates to oligomer formation immediately after formation. Adapting a saturation concentration from Odum *et al.* [21], the authors were able to calculate the evaporation coefficient and determine that SOA partitioning is reversible. However, the model solved used the saturation concentration of a freshly-produced SOA which does not represent the SOA in the smog chamber during the period of the experiment.

Vaden *et al.* [29] induced the evaporation of SOA produced from the ozonolysis of α -pinene by continuously denuding VOC from the chamber by adding activated carbon to the chamber. After 100 minute SOA particles lost 50% of its volume and then 25% of its remaining volume in 1400 minutes. To model the results, the approach employed a seven-product volatility basis set

developed to fit the formation of SOA from α -pinene [24]. Vaden *et al.* iterated the model for a large range of evaporation coefficient, reaching very low values, still the model could not find a value of the evaporation coefficient to fit the experimental results. They attribute the low evaporation rates and the deviation from the theory of rapid reversible partitioning to evidence that the SOA formed has an amorphous state which decreases the diffusion of molecules to the surface of the particle. However, at such large timescales the low evaporation rates could be due to the formation of oligomers, rather than SOA being produced in an amorphous state, during the experiment. Using a volatility basis set that is based on aged SOA would have allowed the model to find a value of the evaporation coefficient to fit the experimental results. Therefore, instead of having bulk diffusion limitations, the thermodynamic limitations might be the cause of the low evaporation rates.

Saleh *et al.* [45] attempted to decouple the thermodynamics from the partitioning kinetics of freshly produced α -pinene oxidized SOA by introducing a temperature step change to the system. The approach introduced a small step change to the system allowing the system to reach equilibrium rapidly after the step change. Using the condensation sink diameter instead of the mass concentration, the particles reached equilibrium when the condensation sink diameter decrease seized after an hour. They calculated the evaporation coefficient to be 0.15 using a volatility distribution derived from their high loading experiments, and accounting for the contribution of vapor by the wall bound particles. The authors concluded that the equilibration time scales recorded, in the range of tens of minutes, for low loading experiments shows that there is no mass transfer resistance.

1.4 Objective

Current investigations are estimating equilibrium timescales and calculating the evaporation coefficient as a method of evaluating the applicability of the absorptive partitioning theory [44, 30, 29]. These approaches are assuming saturation concentrations to model their results from reported literature in data that are not well representing the physical state of SOA being tested. Grieshop *et al.* [44] reported the rapid formation of oligomer for SOA particles in the study, however the evaporation coefficient calculated was based on a vapor pressure derived from Odum's [21] yield data.

In this study, we develop an experimental approach for measuring SOA evaporation and equilibrium time, produced from oxidized gasoline engine exhaust, in a smog chamber. We chose the gasoline engine exhaust as a true contributor for SOA precursors in the atmosphere. We then model SOA evaporation data using mass transfer equations between the surface of a particle and its surrounding, a system not yet studied in literature, using thermodynamic properties calculated from existing techniques instead of assuming values from literature. This model permits us to observe the equilibration time of SOA in the atmosphere and calculate the evaporation coefficient correctly. We can then conclude with confidence whether SOA can attain phase equilibrium in short time scales or whether certain factors, such as mass transfer limitations, hinder or prevent SOA from reaching equilibrium.

Chapter 2

Theory

In our experiments we measure the evaporation of polydisperse SOA in a smog chamber and then model the results to be limited by diffusion from the surface to interface. The model will verify the timescale attained experimentally as well as calculate the evaporation coefficient.

2.1 Evaporation of an Unbounded Aerosol

In the following development of the model we use an adjusted form of Fick's first law of diffusion to fit the experimental results. We first consider the model to solve single particle evaporation in space and then we develop it further to solve for polydispersed aerosol evaporation in an enclosure. Particle evaporation is assumed to be slow evaporation, which involves low concentrations of the diffusing species into the surrounding [46]. Figure 2.1 shows the evaporation process of a particle in a surrounding gas. Particles evaporate to reach a phase equilibrium in a gaseous medium when the surrounding gas concentration reaches the saturation concentration of the particle.

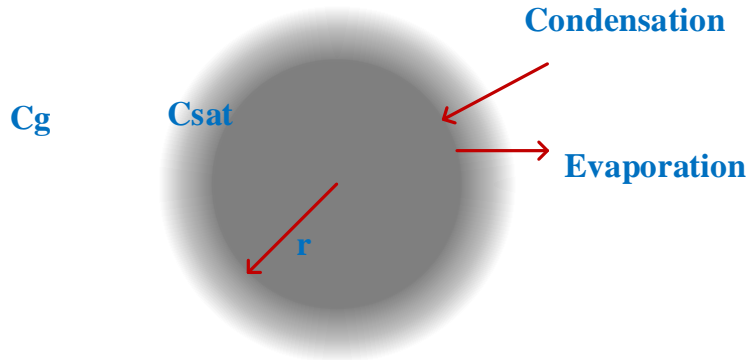


Figure 2.1: The evaporation of a stagnant particle in a surrounding gas. C_g is the gas phase concentration away from the particle, C_{sat} is the vapor saturation ratio, and r is the radius of the particle.

At slow evaporation rates of particles, the interfacial velocities are small and the particles are assumed to be inertia free. Thus, the only mass transfer mode is that of diffusion. The temperature between the particles and the surrounding are not too large when the particle is at a temperature below the boiling point. The partial pressure of vapor is small and the physical parameters of the gas such as density and diffusivity are constant [46]. The molar flux of a species through stagnant air can be described by Fick's first law of diffusion in dilute conditions according to Equation 2.1.

$$J_{A,r} = -D_{SOA,Air} \frac{dr}{dC} \quad (2.1)$$

where $J_{A,r}$ is the molar flux of SOA at any radius, $D_{SOA,Air}$ is the diffusion coefficient of SOA in air, r is the particle radius, and C is the concentration of SOA in the particle phase. The Maxwellian flux equation derived from Equation 2.1 that describes the diffusion as a function of concentration at the surface and away of the particle is given in Equation 2.2 [47].

$$\frac{dC}{dt} = 2\pi r D_{SOA,Air} (C_g - C_{sat}) \quad (2.2)$$

In Equation 2.2 C_{sat} is the saturation concentration of SOA vapor at the particle surface and C_g is the concentration of SOA vapor far from the particle surface. To describe the change in particle size, Equation 2.3 can be used instead of concentration change in Equation 2.2.

$$\frac{dr}{dt} = 2\pi r D_{SOA,Air} (C_g - C_{sat}) \quad (2.3)$$

Equation 2.4 solves the change in particle diameter ($d(d_{p,i})$).

$$\frac{d(d_{p,i})}{dt} = \frac{-4D_{SOA,Air}(C_{sat} - C_g)}{\rho d_{p,i}} \quad (2.4)$$

Equations 2.2 and 2.4 solve evaporation that occurs in the continuum regime as described by the Maxwell Equation for mass diffusion. The transport regime, whether continuum, transition, or free molecular regime, is defined by the ratio of the mean free path (λ) of a molecule and the diameter (d) of the particle which is Knudsen number ($Kn = \frac{2\lambda}{d}$). The application of the transition flow regime is dictated by the knudsen number range $0.1 \leq Kn \leq 10$. The mean free path (λ) of the particle is defined as the ratio between the diffusion coefficient of the molecules in the gas phase (D) and the mean molecular speed (\bar{c}) is defined as follows:

$$\bar{c} = \sqrt{\frac{8RT}{\pi M}} \quad (2.5)$$

$$\lambda = \frac{3D}{\bar{c}} \quad (2.6)$$

Where M is the molecular weight of SOA, R is the ideal gas constant, and T is

the temperature of the system. SOA, when produced, has a size range of particle diameters between $30nm$ and $500nm$ in its population distribution, the range of knudsen numbers for the polydisperse distribution is between 0.28 and 4.67. Thus the mass transfer is solved in the transition regime.

In the transition regime, the molecule has to travel long distances to collide with a particle after which it either reflects or impinges on the surface of the particle [46]. A correction factor is introduced to the Maxwell diffusion equation to interpolate the results between the continuum regime and the free molecular regime. In this regime the flow of particles to the surface is governed by both gas phase diffusion far from the particle and surface kinetics at the surface of the particle described by the interpolation factor. Fuchs and Sutugin [48] formulated Equation 2.7 as the interpolation factor C_m . The evaporation coefficient accounts for the surface kinetics and the gas phase diffusion coefficient for the diffusion far from the particle. Lower evaporation coefficients than unity are due to retardation of evaporation in the transition regime due to intermolecular collisions at the interface during the desorption of a molecule. Molecules emitted from the surface may collide with a vapor molecule and reflect back to the particle, molecules may collide with a vapor molecule and re-emitted to the surrounding gas phase[49], Figure 2.2 illustrates the interactions occurring at the surface of the particle.

$$C_m = \frac{1 + Kn}{1 + (\frac{4}{3\alpha} + 0.377)Kn + \frac{4}{3\alpha}Kn^2} \quad (2.7)$$

Thus, Equations 2.2 and 2.4 become:

$$\frac{dC}{dt} = 2\pi d_{p,i} D_{SOA,Air} C_{m,i} (C_g - C_{sat}) \quad (2.8)$$

$$\frac{d(d_{p,i})}{dt} = \frac{4\pi D_{SOA,Air} C_{m,i}}{\rho_p d_{p,i}} (C_g - C_{sat}) \quad (2.9)$$

where ρ is the particle density and α is the evaporation coefficient. The evaporation coefficient is empirically calculated through comparing predicted evaporation rates and the observed evaporation rates. The evaporation coefficient is equal to the accommodation coefficient which was first introduced by Maxwell [50] in his study of particle condensation, it is defined as the probability of a molecule colliding with a surface that will impinge on the surface instead of reflecting back to the surrounding.

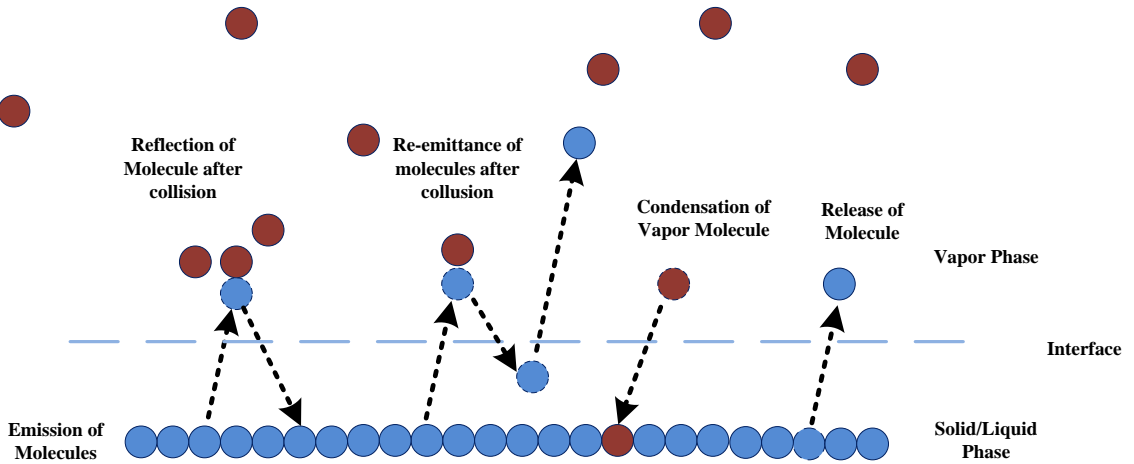


Figure 2.2: The interactions of the molecules occurring at the interface of a particle, molecules may collide with other molecules or released immediately to the surrounding gas.

2.2 Particle Evaporation in an Enclosure

This section moves the model from a single SOA particle evaporating in gas to a parcel of SOA particles in a smog chamber. SOA particles evaporating in a smog chamber include additional physical interactions than what was discussed above. In the chamber, particles and vapors partition to the walls, and those species contribute to the equilibrium between the SOA particles and the vapor phase. In this current study, volatile organic compounds adsorption to the walls is neglected. Figure 2.3 illustrates the interaction of polydisperse SOA particles in the smog chamber.

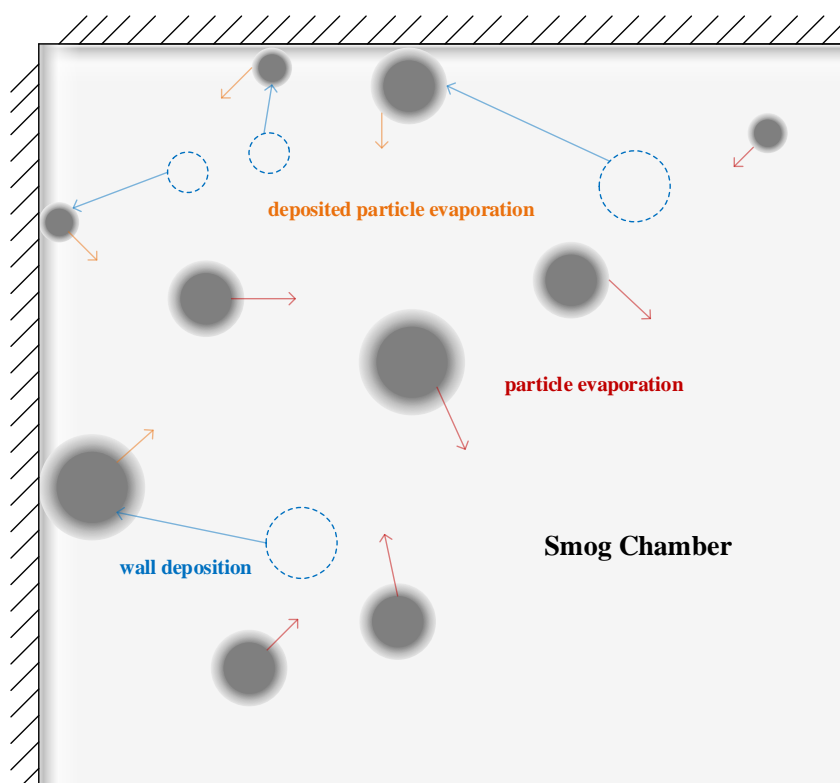


Figure 2.3: Particle interaction in the smog chamber. The considered interactions are deposition of the particles on the chamber walls, the evaporation of particles to reach equilibrium and the evaporation of deposited particles on the walls

Moving away from Equations 2.8 and 2.9 of particles evaporating in an infinite space, the evaporation of particles in a chamber requires accounting for the contribution of all sources of gas phase molecules. The mass balance for gas phase molecules in the differential form for a closed system chamber is shown in Equation 2.10.

$$\frac{dC_g}{dt} = \left[\frac{dC_g}{dt} \right]_{sus} + \left[\frac{dC_g}{dt} \right]_{deps} \quad (2.10)$$

The rate of evaporation of particles, and thus the increase in gas phase concentration, either deposited on the walls or suspended in the enclosure is solved using Equation 2.8. However, deposited particles will not evaporate at the same rate as other particles. Thus a factor ω is introduced to the rate of evaporation of particles deposited to the walls. Equations 2.11 and 2.12 are the rates of evaporation.

$$\left[\frac{dC_g}{dt} \right]_{sus} = -2\pi d_{p,i} DC_m N_{sus,i,t} (C_{sat} - C_g) \quad (2.11)$$

$$\left[\frac{dC_g}{dt} \right]_{deps} = -2\pi d_{p,i} DC_m (\omega \cdot N_{wall,i,t}) (C_{sat} - C_g) \quad (2.12)$$

where $N_{wall,i,t}$ is the number concentration of particles that are lost to the chamber walls for a specific diameter i at any time t and $N_{sus,i,t}$ is the number concentration of particles that are suspended in the enclosure for a specific diameter i at any time t in a distribution spanning n diameters. In addition to Equation 2.10 the diameter change equation will be solved simultaneously. Equation 2.13 is the expanded mass balance equation for concentration change.

$$\frac{dC_g}{dt} = -2\pi D \sum_{i=1}^n d_{p,i} C_m (C_{sat} - C_g) (N_{sus,i,t} + \omega \cdot N_{wall,i,t}) \quad (2.13)$$

The number for suspended and lost concentrations can be calculated according

to equations 2.14 and 2.15, derivation of this Equation can be found in [51]:

$$N_{wall,i,t} = N_{sus,i,o} - N_{sus,i,o}exp(-\beta_i t) \quad (2.14)$$

$$N_{total,i,t} = N_{sus,i,t} + N_{wall,i,t} \quad (2.15)$$

where $N_{total,i,t}$ is the total suspended number concentration of particles of a specific particle diameter at any time t , $N_{sus,i,o}$ is the initial number concentration in the enclosure, and β_i is the deposition coefficient specific to each particle diameter. The total number concentration of SOA suspended or deposited particles can be calculated as $N_{j,total} = \sum_i N_{j,i}$.

Similar to other model approaches [52, 53, 45, 54], condensation sink diameter is used to understand the change in particle sizes. Condensation sink diameter (d_{cs}) is a concept introduced by Lehtinen *et al.* [55] to assign a diameter of a monodisperse aerosol with the same net evaporation rate as the polydisperse aerosol when the number concentration is equal.

The condensation sink is $CS = 2\pi D_{SOA,Air} \sum C_m d_{p,i} N_i$ and the condensation sink diameter for a certain number distribution is:

$$d_{cs} = \left(\frac{\sum_{i=1}^n N_i d_{p,i}^a}{\sum_{i=1}^n N_i} \right)^{\frac{1}{a}} \quad (2.16)$$

Where a is a size-dependent value for the growth exponent approaching 2 for small particles in the free-molecular regime. The condensation sink of each particle number concentration are given in Equations 2.17 and 2.18.

$$CS_{wall} = 2\pi D d_{cs} \sum_{i=1}^n C m_{i,t} N_{wall,i,t} \quad (2.17)$$

$$CS_{sus} = 2\pi D d_{cs} \sum_{i=1}^n C m_{i,t} N_{sus,i,t} \quad (2.18)$$

The condensation sink of the particles has a unit of (s^{-1}) provides a measure of the rate of evaporation of suspended particles and the rate of evaporation of deposited particles separately.

Finally, the equations predicting the gas phase concentration (Equation 2.20) and the change particle condensation sink diameter (Equation 2.19) are given below:

$$\frac{d(d_{cs})}{dt} = \frac{-4DC_m}{\rho_p d_{cs}} (C_{sat} - C_g) \quad (2.19)$$

$$\frac{dC_g}{dt} = (CS_{sus} + \omega CS_{wall})(C_{sat} - C_g) \quad (2.20)$$

2.3 Equilibrium Approach

The approach we use in the experimental procedure is an equilibrium perturbation approach, resembling the approach of Saleh *et al.* [45]. Saturation ratio (SR) of the parcel of SOA in an enclosure is ratio between the gas phase concentration in the enclosure at any point in times and the saturation concentration of the particles. Evaporation of the particles is induced by decreasing the gas phase concentration and thus changing the saturation concentration, from its equilibrium at a saturation ratio of 1 as shown in figure 2.4. We transfer SOA particles formed in the reactor at steady state having $SR = 1$ to a larger volume vessel with pure air; the approach we use in the experiment, however, differs from that of *et al.* [45] in the method of perturbation. The perturbation method used in the previous study uses SOA from a biogenic precursor and perturbs equilibrium by a thermal step change, while in our study we

use an isothermal dilution step change in the chamber for SOA produced from anthropogenic SOA. The chamber acting as a batch vessel has no SOA prior to filling, ensured by continuous flushing for 36 hours. Equilibrium of particles in the reactor is perturbed and the saturation ratio decreases to a value less than 1. Particles in the chamber evaporate to increase the gas phase concentration and regaining equilibrium when the gas phase concentration is equal to the saturation concentration of the particles.

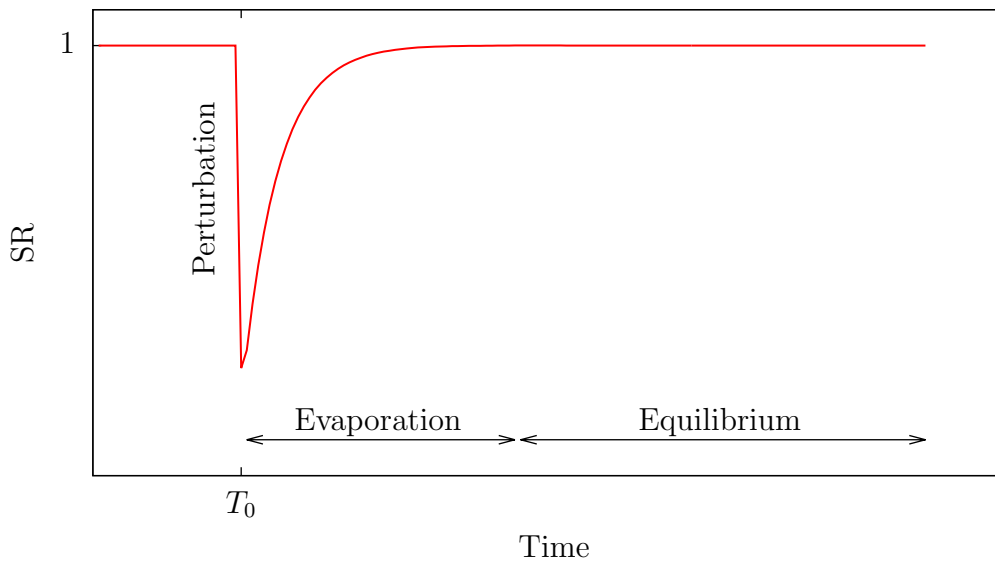


Figure 2.4: Change in saturation ratio throughout the experiment, from PAM to the smog chamber

The evaporation rate and the journey of particles to equilibrium allows us to follow the equilibrium trend and calculate the evaporation coefficient. However while particles regain equilibrium in the chamber by evaporating, particles are also depositing to the walls of the chamber changing the size distribution of the aerosols in the chamber. As mentioned in Chapter 2, we use

the condensation sink diameter equilibrium profile for fitting the results. The equilibrium profile is then corrected for wall loss deposition; the corrected equilibrium profile of particles travelling from an $SR < 1$ to $SR = 1$ is then fitted to the results of the evaporation equations to calculate the optimum value of the evaporation coefficient to minimize the fit error.

Chapter 3

Materials and Methods

This section describes the experimental setup, the experimental procedure to collect data results and the code of the evaporation model to find an optimum evaporation coefficient to minimize the error of the experimental results fit.

3.1 Experimental Setup

In our experimental approach we produce SOA through a photochemical oxidation reaction from diluted gasoline engine exhaust in a continuous flow reactor. We then dilute the oxidized products by transferring the particles to a smog chamber and observe the partitioning of SOA, a schematic of the process is shown in Figure 3.1.

The gasoline engine is a single cylinder unit supplying a maximum power of 1 kVA. A rotating disk diluter (Matter Engineering, Model MD19-3E) dilutes the exhaust. Unlike other approaches that utilize the smog chamber for both producing SOA and observing the desired SOA behavior [56, 22, 23, 57, 58, 59], we adopt the potential aerosol mass (PAM) method introduced by

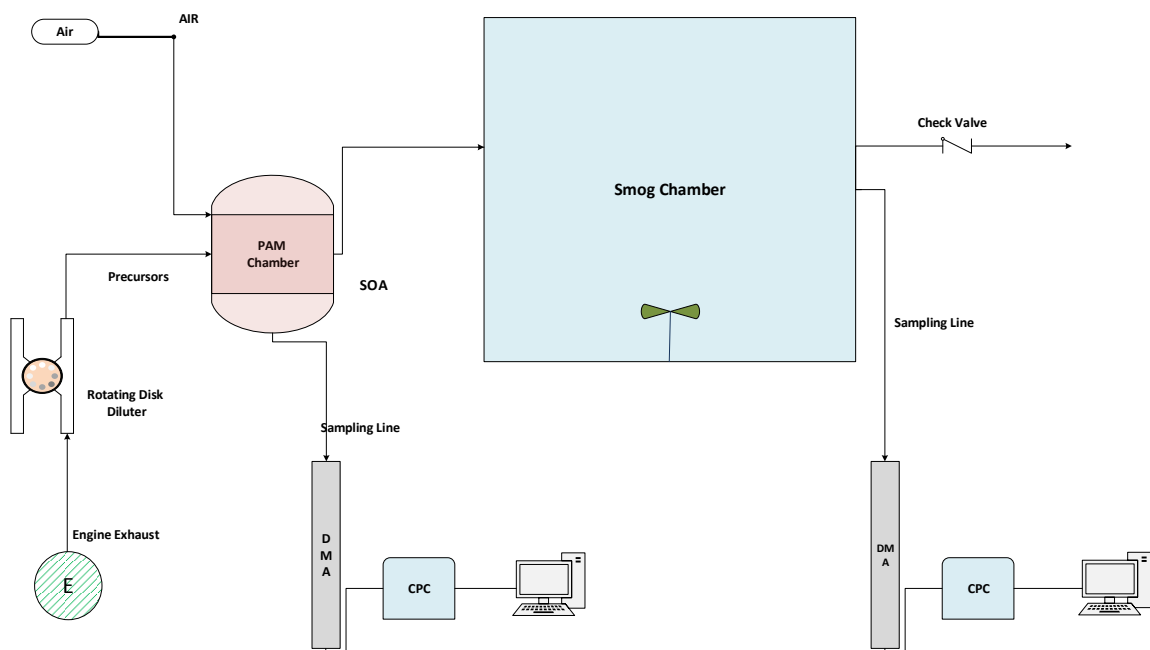


Figure 3.1: Process flow diagram. The PAM is the potential aerosol mass reactor, the CPC is the condensation particle counter, the DMA is the differential mobility analyzer and E is the gasoline engine

Kang *et al.* [60] to use a simple continuously stirred flow reactor to produce SOA in short residence times. Hereafter the SOA production reactor is named the PAM chamber, made of stainless steel of a 64 L volume. We produce SOA in the PAM chamber and not in the smog chamber because of its ease of control and short residence times.

In the PAM chamber, a UV mercury lamp (BHK Inc) and a fan are installed to initiate the radicalization of OH molecules and ensure well-mixed conditions respectively. The light wavelengths emitted by the UV lamp are 185 nm and 254 nm. The 185 nm wavelength produces ozone and 254 nm wavelength produces hydroxyl radicals [7].

The smog chamber is a 4.9m^3 (1.7 m side length) cubic bag made of 5 mil perfluoroalkoxy alkane (PFA) manufactured by Welch fluorocarbon. The chamber is equipped with eight ($\frac{1}{4}$ ") and two (1") Kenyar fittings for input and output ports and an (8") slit. To avoid particle stratification, the smog chamber has a fan resting on the middle of its bottom surface to ensure well mixed conditions. The smog chamber is hereafter called the chamber. The fan inside the chamber was coated with Teflon tape to minimize adsorption to the surfaces. Temperature and humidity are measured and logged continuously by a temperature and humidity probe (Vaisala, Model HMP60) suspended from an outlet port close to the wall of the chamber.

Throughout the production in the PAM chamber and evaporation in the chamber the mass, number, diameter, surface and volume distribution and total concentrations are measured continuously using two scanning mobility particle sizer (SMPS) having a differential mobility analyzer (DMA, TSI, Model 3081) and a condensation particle counter (CPC, TSI, Model 3772). The sheath flow to aerosol flow is 4:1 and the voltage spans a range of 42V - 9470V to measure a diameter range of 25nm till 514nm.

3.2 Experimental Procedure

We operate the gasoline engine at zero load, filled with unleaded octane grade 98 gasoline purchased from local gas stations. The engine's exhaust is transferred through a heated line at 120°C to the rotating disk diluter where the exhaust is diluted 3000 times (maximum potentiometric setting in the diluter) with activated carbon filtered HEPA filtered air. The output of the diluter is a 5 L/min mixture of exhaust diluted with filtered air comprising the

precursor line to the continuously stirred reactor.

The precursor line is further diluted in the PAM chamber by a 30 L/min activated carbon filtered HEPA filtered air. The airflow inside the chamber acts as a diluent to the SOA concentrations at steady state, thus governing the concentration produced by the PAM chamber by the air flowrate. We start oxidation by turning on the UV lamp. When the exhaust oxidation reaction reaches steady state as observed by stagnation in the mass concentration of the aerosol particles measured by the SMPS, the outlet flow of the PAM chamber is connected to the smog chamber. This step serves as an isothermal dilution step, where SOA is transferred from high concentrations saturated conditions to a 5m^3 volume filled with filtered air.

The chamber is designed to operate as a batch to observe the decay in particle mass concentration due to evaporation of SOA over a period of time using one SMPS. We fill the chamber with the freshly produced SOA from the PAM chamber, while continuously observing the concentration to stop filling the chamber at the desired number or mass concentration. When SOA is transferred from the PAM chamber, high SOA concentration medium, to the chamber, low SOA concentration medium, evaporation is induced. In this experiment, the concentration set point is approximately $10\mu\text{g}/\text{m}^3$. Our starting mass concentration is compatible with other smog chamber experiments with low particle loading, where the mass concentration is kept at a low value ($\leq 10\mu\text{g}/\text{m}^3$) [45]. In addition to that, the number concentration is kept at low values ($\leq 20000\#/\text{cm}^3$) to avoid coagulation [61, 51, 28]. The experiment proceeds by continuously measuring the particle decay for several hours.

Before each experiment, we continuously flush the chamber with 30L/min of activated carbon filtered HEPA filtered air for more than 36 hours for two

purposes. This is done, to remove residual suspended particles from the current experiment and to force deposited particles on the walls of the chamber to evaporate by continuously perturbing its equilibrium with the surrounding. At the onset of each new experiment, the mass concentration is less than $0.009\mu\text{g}/\text{m}^3$ and the number concentration is less than $10 \text{ \#}/\text{cm}^3$. Temperature in the chamber is not controlled and instead is governed by the ambient conditions of the lab where the chamber is suspended in. Temperature variability between experiments on different days is less than one degree Celsius.

3.3 Experimental Conditions

We have performed four experiments to calculate the evaporation coefficient. Table 3.1 shows the following experimental variables at each experimental run: the average production concentration of SOA (C_{PAM}), the filling flowrate from the PAM chamber to the chamber ($F_{filling}$), the time required to fill the chamber ($T_{filling}$), the volume of gas (V_{filled}) added to the smog chamber initially filled with pure air at 5m^3 to constitute a step change, and the dilution ratio (DR). The dilution step change occurs when transferring SOA from the PAM chamber to the smog chamber as discussed in section 2.3, the SOA concentration in the smog chamber initially are listed in table 3.2. Based on that, the dilution ratio is calculated as the ratio between the SOA concentration in the PAM chamber and the smog chamber and the dilution time step is the required time to transfer SOA from the PAM chamber to the fill the smog chamber ($T_{filling}$). The initial conditions of SOA for the four experiments in the chamber are listed in table 3.2. The initial conditions referred in the text are those of the conditions in the chamber after filling at the onset of particle

decay at T_0 as shown in figure 2.4.

Table 3.1: The initial conditions of the four SOA evaporation experiments

Experiment	C_{PAM} ($\mu g/m^3$)	$T_{filling}$ (<i>min</i>)	$F_{filling}$ (<i>LPM</i>)	V_{filled} (<i>L</i>)	DR
A	60	28	32	896	5
B	140	18	33	594	13
C	97	20	43	860	9
D	76	26	34	884	7

Table 3.2: The initial conditions of the four SOA evaporation experiments

Experiment	N_o ($\#/cm^3$)	M_o ($\mu g/m^3$)	Dcs_o (<i>nm</i>)	Temperautre (<i>K</i>)	RH (%)
A	15610	10.6	99.4	25	12
B	18800	10.1	94	22	15
C	22161	10.1	88.1	23	13
D	14861	9.6	99.07	22	12

3.4 Methods

Throughout the experiment we continuously measure the SOA population concentrations in the chamber. This will later allow us to study the response of the particles after dilution. The SMPS measures the number distribution of particles and then calculates the subsequent volume, mass, and sur-

face area distributions. The size distributions are a function of the diameters of the particles, as shown for number and volume distribution in Figure 3.2 for a typical starting SOA distribution in the chamber. At each time step, defined as 60 seconds, the SMPS scans the continuously withdrawn samples of SOA from the chamber and reports the concentration of the particles. The software simultaneously converts the number concentration over each size interval to mass, volume, diameter and surface area. At the end of each time step the software then calculates the total particle concentration by summing the particle concentration at size interval, along with other properties.

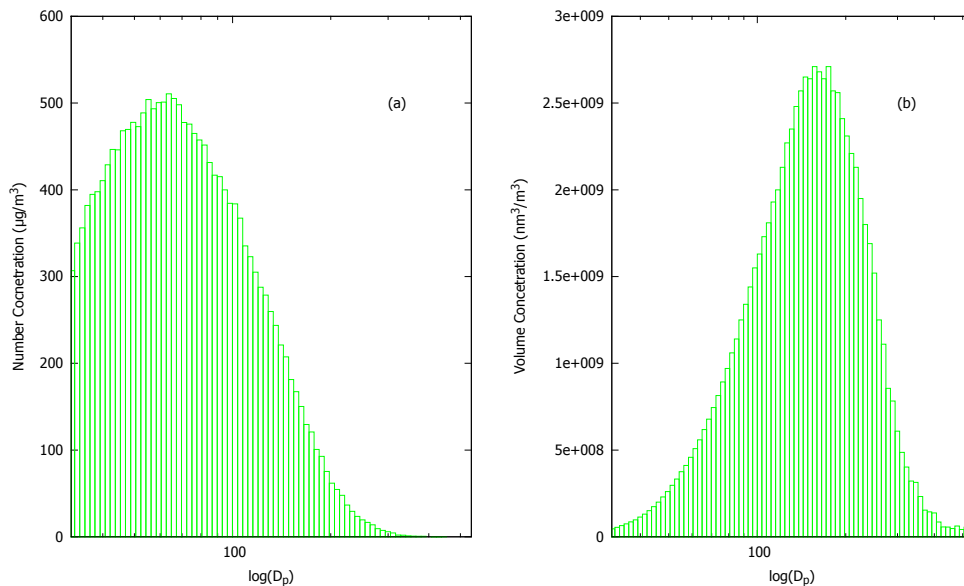


Figure 3.2: Typical particle size distribution of SOA in the chamber after isothermal dilution for (a) Number distribution (b) Volume distribution

The total number and volume concentrations decrease due to the two governing processes in the chamber: (1) evaporation and (2) particle loss to the walls of the smog chamber. Evaporation of particles shifts the number and volume particle size distribution while it has no effect on the total number con-

centrations. However, particle wall loss causes a shift in the size distributions as well as decreasing the total number and volume concentrations.

We represent our number distribution with a single property to observe its response to evaporation. As mentioned Chapter 2 we use the condensation sink diameter as our representation property. The condensation sink diameter is a property that allows the calculation of the evaporation rate of a monodisperse aerosol having the same polydisperse aerosol evaporation rate at the same number concentration [55], which makes the use of this property over other diameter representation properties desirable. As with other diameter representation, the condensation sink diameter a property dependent on changing size distribution, and both evaporation and wall loss change the size distributions. Figure 3.3 shows the simulated behavior of an SOA population and the calculated condensation sink diameter according to evaporation and wall loss separately. Wall loss increases the condensation sink diameter because the smaller diameters are disappearing from suspension while the evaporation decreases the condensation sink diameter due to a decrease of the size of the particles.

Figure 3.4 is a plot of the typical results of a certain experiment performed. The plot shows the condensation sink diameter initially decreasing due to evaporation and when evaporation rate decreases, the mode of change shifts to particle deposition which causes a monotonic increase towards larger diameter. After confirming that in our smog chamber the wall loss rate is size dependent we can then account for the particles that deposit on the walls throughout the experiment. Through the represented property, the condensation sink diameter, we linearly fit the increasing in the diameter and then subtract the slope of increase from the entire data set. This simple approach to correcting the condensation sink diameter ensures that the correction parameters share

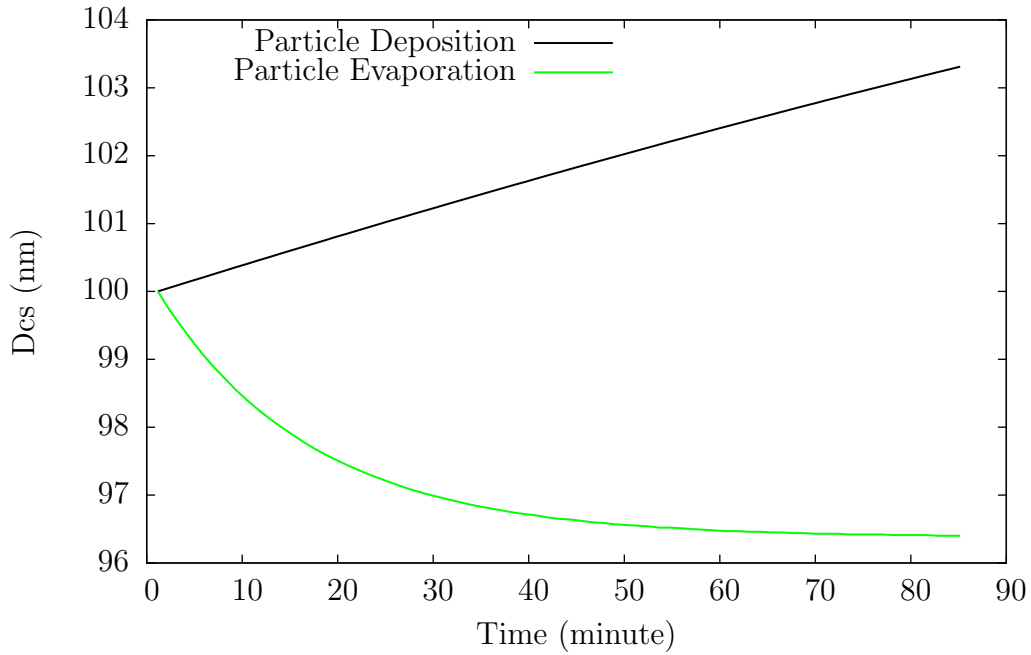


Figure 3.3: The simulated trend of change of the condensation sink diameter governed by particle loss and evaporation separately

the same experimental conditions as the temperature, humidity and pressure. Thus, removing an uncertainty factor while calculating the evaporation coefficient. Figure 3.4 plots the condensation sink diameter after correcting the measured results, showing particles decreasing due to evaporation and then reaching equilibrium after a period of time.

In addition to loss of particles, particles adhering to the walls of the chamber may contribute to the evolution of the gas phase concentration. The nature of deposition may play a role in defining the wall-suspension partitioning coefficient (ω), in general particles on the walls may evaporate at the same rate as the suspended particles, at a lower rate, or they may not evaporate at all. Thus the factor ω is introduced to account for the contribution of lost particles to the gas phase concentration. An assumption of $\omega = 1$, modeled as if

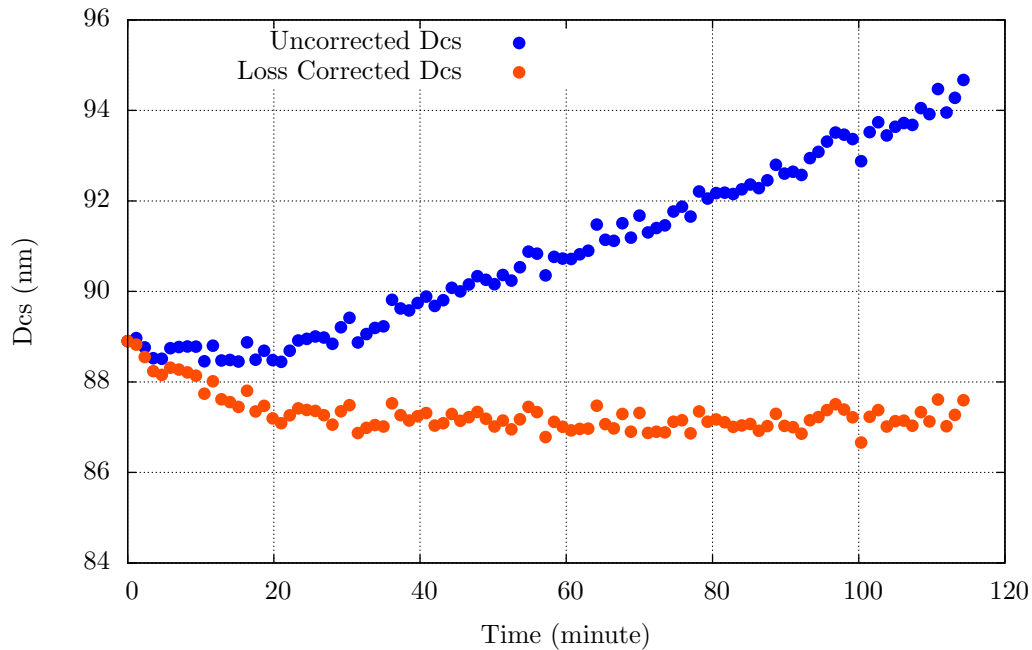


Figure 3.4: The typical result of a corrected condensation sink diameter and the uncorrected condensation sink diameter.

the chamber has no walls, corresponds to the case where the initial number of particles is evaporating throughout the experiment. This assumption will lead to an underestimated value of the evaporation coefficient. An assumption of $\omega = 0$, corresponds to the case when particles penetrate the walls and are lost forever. This assumption will lead to an overestimated value of the evaporation coefficient. We will address the effect of the ω on the evaporation coefficient in Chapter 4.

3.5 Code Description

After processing the results and calculate the equilibrium profile of SOA, we send these results to the model and calculate a fit for the results.

We use the Aerosol Research Lab (ARL) evaporation code, which was used in

previous publications [52, 62, 63] for thermodenuder (TD) experiments. We adapted the code to model our chamber results. The code calculates the optimum evaporation coefficient based on fitting the corrected experimental results, by simulating the evaporation of a parcel of SOA loaded initially in a smog chamber. We solve in MATLAB the two differential equations 2.19 and 2.20 using the ODE45 solver for non-stiff systems. In addition to solving the mass transfer differential equations, the code accounts for particle losses to the walls of the chamber. The differential equations described in the previous section are solved simultaneously, at each time step defined by the user.

The equations in the code solve for the evaporation of a number concentration of particles in which a portion of that concentration, contributing to the increase in the gas phase concentration, are particles deposited onto the walls of the smog chamber. This concentration is calculated by the experimentally derived rate of SOA particle loss rate. By using the SOA total loss rate we remove one uncertainty from our calculations regarding particle deposition.

The saturation concentration is an important physical parameter in the evaporation model. However, there is no direct method to determine the saturation concentration from the experimental results and we do not measure the gas phase concentration in the chamber during the experiment. With the absence of particle losses, the saturation concentration can be calculated as the mass transferred from the particles to the gas phase. But, particle deposition and their contribution to the gas phase concentration impose complications on applying a comprehensive mass balance. Thus, we use the same algorithm used for determining the evaporation coefficient to determine the a minimum estimate of gas concentration needed to achieve the equilibrium change in the condensation sink diameter.

The only uncertainty considered to be involved in reporting the change in particle sizes arises from the 3% error from electrostatic classification of particles [64]. We avoid uncertainties reported in literature [65, 66, 67] while using a size-dependent loss rate for account for wall deposition in the measured size distributions, by using the linear fit of the increase in the condensation sink diameter to account for loss of particles. The propagation of uncertainty in measurements to the evaporation coefficient is then calculated using a sequential perturbation method through a Monte Carlo simulation integrated in the code.

The Monte Carlo scheme simultaneously changes the number distribution by a random factor (ϕ) in the range of [-1 1] of its error (u_x). The number concentration in the distribution at each point in time is varied according to equation 3.1.

$$N_{i,t}^{per} = N_{i,t}^{average} + \phi u_x \quad (3.1)$$

The factor ϕ is generally negative or positive so that the independent variable ϕu_x is either less or greater than the average independent variable error. After perturbing each number concentration of each size range, the perturbed condensation sink diameter is calculated of the experimental results. At the end, the simulation converges to the optimum evaporation coefficient when the difference between the predicted results and experimental results is less than a predefined error [68].

After defining the error in measurements and the saturation concentration, the code calls the perturbed experimental results at each iteration to calculate a fit between the predicted and observed results. Table 3.3 lists the physical parameters the code receives to proceed with calculations, this will

serve as a base case for reporting the results and we will further deviate from this base case to explore the effects of changing the gas diffusion coefficient and the molecular weight on the evaporation coefficient.

Table 3.3: Physical Parameters used in the evaporation model for the base case calculations

Physical Parameter	Unit	Value
Molecular Weight of SOA	<i>kg/mol</i>	0.15
Gas Diffusion Coefficient	<i>m²/sec</i>	5.10 ⁻⁶
Molecular Weight of Air	<i>kg/mol</i>	0.029
Density of SOA	<i>kg/m³</i>	1400

The flowchart in Figure 3.5 shows the algorithm of the code employed to calculate the best fit value of the evaporation coefficient. The code first receives the experimental results of a certain experimental run. A 100 sets of perturbed condensation sink diameters for the uncertainty in particle size measurements are calculated based on the perturbed number distributions. The algorithm then calculates the corresponding saturation concentration for each perturbed set of equilibrium profile of the condensation sink diameter. When all the conditions are calculated, we provide the code with a range of evaporation coefficients [0 1] to evaluate the response of the code, the code solves the mass transfer differential equations at each iteration of the Monte Carlo simulation and value of evaporation coefficient. The number of iteration is then the quotient of the number of Monte Carlo simulation and the length of the array of the evaporation coefficient. Using a brute force algorithm.

At each iteration, the model solves the differential equations and compares the results to the perturbed condensation sink diameter set. Using the

brute-force search algorithm the results are recorded as the optimal value if the difference between those two is less than an error defined by the user and the corresponding evaporation coefficient is saved as optimum. For each perturbation simulation a value of the evaporation coefficient is recorded in an array. At the end of the user defined number of Monte Carlo simulations, the optimum evaporation coefficient selected is the average of the array of coefficients calculated at each perturbation simulation and the standard deviation is reported as the error propagated from the uncertainties accounted for in the code.

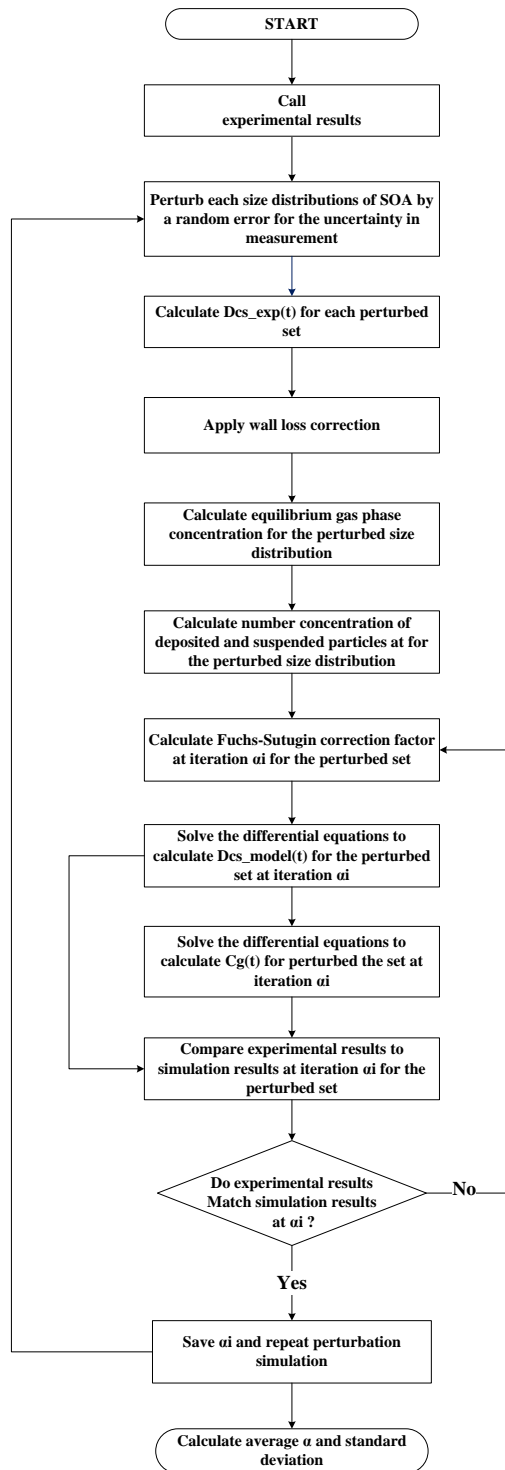


Figure 3.5: Evaporation model code algorithm

Chapter 4

Results

We present the results of the isothermal dilution experiment of SOA evaporation of at atmospheric-relevant concentrations. The initial conditions of SOA evaporation at the onset of evaporation after dilution of the four experiments performed are listed in Table 3.2. Figure 4.1 shows the equilibrium profile for the condensation sink diameter corresponding to experiments A, B, C, and D introduced in Table 3.2.

Although we witness some scatter in the data as a function of time, we determine the equilibrium state of SOA particles when the change in the condensation sink diameter is constant, relative to the starting diameter. At that point the saturation concentration is calculated as described in Chapter 3. The evaporation model calculated the evaporation coefficient based on the best fit between the observed profile and the predicted profile. Table 4.1 lists the optimum value of the evaporation coefficient for experiments A, B, C, and D, the uncertainty accompanied, and the saturation concentration at an ω of 1. The evaporation coefficient lies within the range of [0.01 0.1]; we attribute the slight variability in the evaporation coefficient to the uncontrolled temperature and

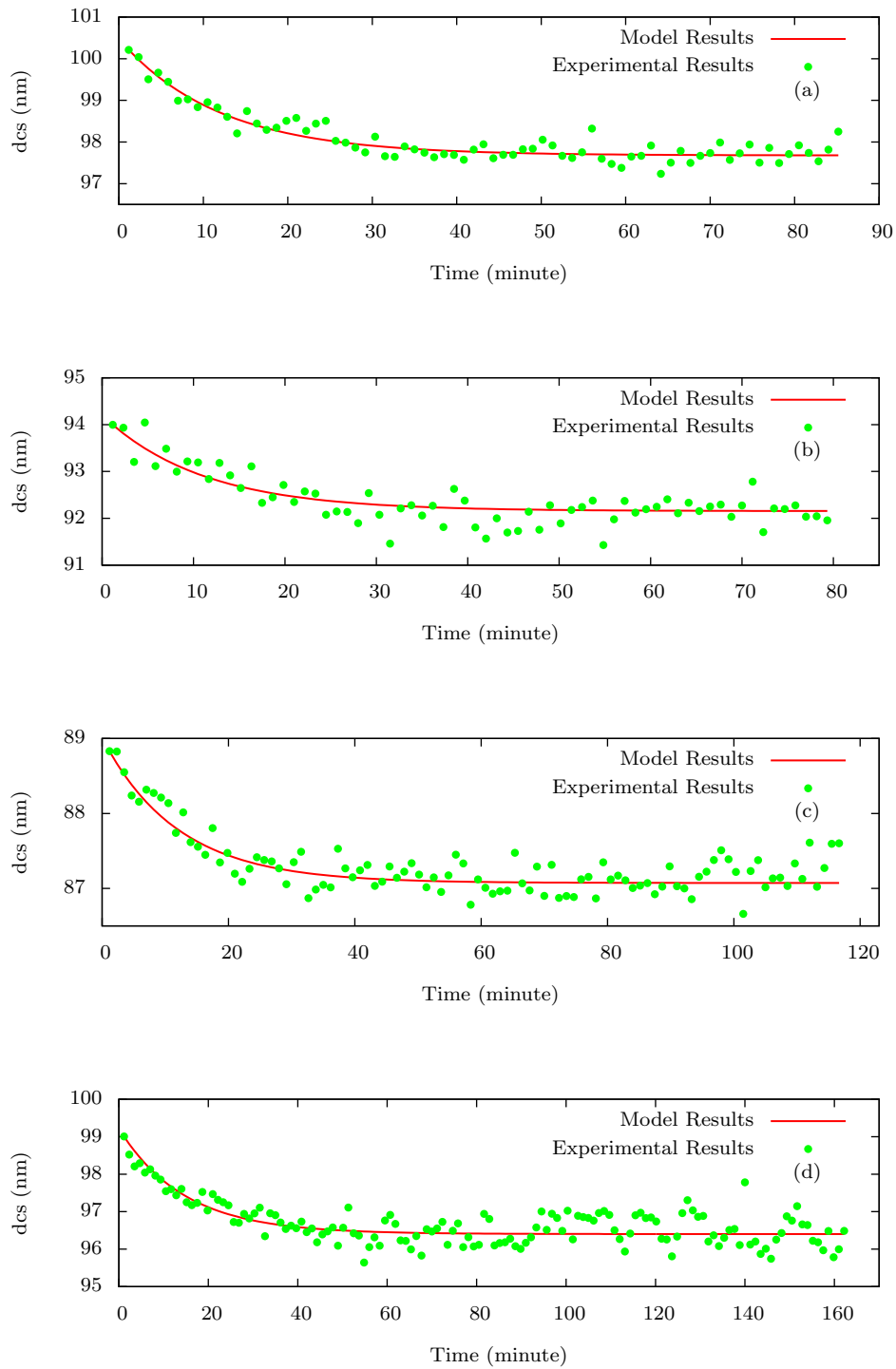


Figure 4.1: The equilibration profile of the condensation sink diameter measured over time for the four experiments (a) experiment A, (b) experiment B, (c) experiment C, (d) experiment D

wind flow conditions around the smog chamber.

Table 4.1: The calculated results of the evaporation coefficient, the saturation concentration and equilibration time from the evaporation model

Exp	$C_{sat}(\mu g/cm^3)$	$dDcs(\%)$	α	τ
A	0.75	2.53	0.065 ± 0.00311	11.166
B	1.01	1.96	0.065 ± 0.00149	13.793
C	0.81	1.91	0.063 ± 0.00431	11.153
D	1.32	2.63	0.059 ± 0.00199	13.961

The characteristic timescale (τ) or the e-folding time, defined as the time for particles to approach equilibrium concentration of their evaporation response after perturbation [69, 70], is on average 12.5 minutes. The evaporation model also calculates the evolution of gas phase concentration over time, we represent this concentration as a non-dimensional value of C_g/C_{sat} signifying the saturation ratio (SR) of the system at the onset of dilution and till the system reach equilibrium at $SR = 1$. Figure 4.2 shows the calculated SR evolution over time for experiment A where $\alpha = 0.063$. In the figure also we plot the corresponding evolution of saturation ratios at different evaporation coefficient values to that only one value of the evaporation coefficient will meet the evaporation profile corresponding to the experimental results.

The assumption of the reversibility of wall losses and the subsequent assumption of a wall-suspension partitioning coefficient adds an additional uncertainty parameter into our study. Currently, there is not one value of the coefficient enjoying consensus, Stanier *et al.* [32], used a value of 0.25, Loza *et al.* [43] used a value of 1 and Saleh *et al.* [45], determined the value to be 0.3, Weitkamp *et al.* [71] uses $\omega=1$ and $\omega=0$ as limiting cases. In Figure 4.3 we

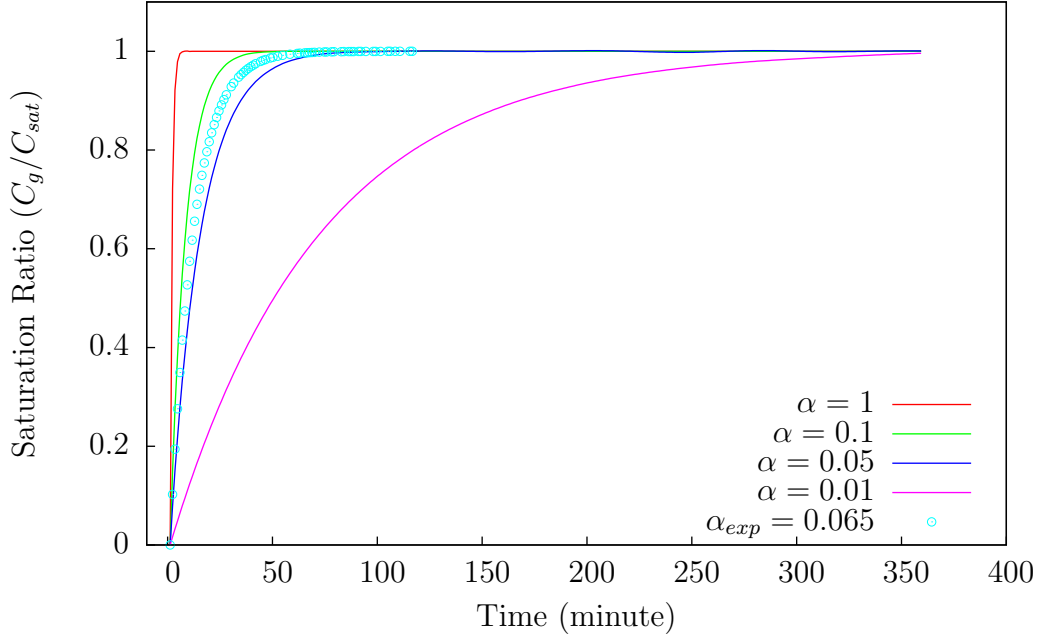


Figure 4.2: The rise in the saturation ratio during evaporation simulated at different evaporation coefficient values, and the result calculated from experiment C

present the evaporation coefficient at each experiment calculated for the values of 0, 0.2, 0.5, 0.7, and 1.

The calculated evaporation coefficients decrease with increasing ω , increasing ω signifies an increasing number of particles contributing to the equilibrium. Because the evaporation coefficient does not change beyond the range of [0.01 0.1] in the remaining we use the calculated evaporation coefficients at 0 and 1 to demonstrate our results.

We also examined the effect of varying the adopted values of the molecular weight and the gas diffusion coefficient in our base case on the evaporation coefficient. The base case used for reporting all the results, had a molecular weight and diffusion coefficient of $M = 150g/mol$ and $D = 5 \times 10^{-6}m^2/sec$ respectively. In comparison to our used parameters Shiraiwa *et al.* [72] used the

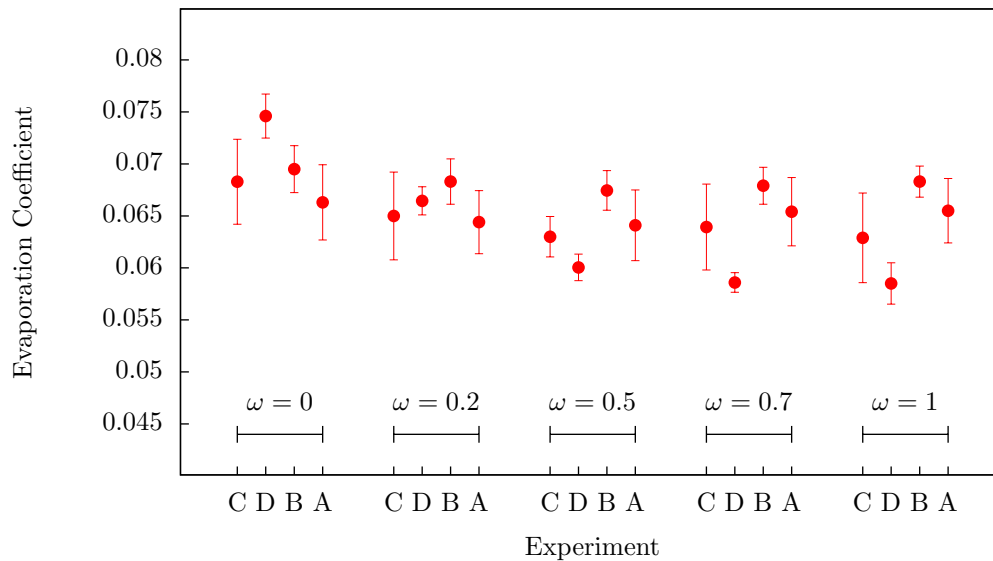


Figure 4.3: The variation of the individual evaporation coefficient of each experiment at selected ω values

values $M = 100g/mol$ and $D = 1 \times 10^{-5}m^2/sec$, while Saleh *et al.* [45] used the values $M = 200g/mol$ and $D = 5 \times 10^{-6}m^2/sec$. In Figure 4.4 we show the variation of the evaporation coefficient according to a range of M. Freshly formed SOA particles have low M and aged SOA particles have high M due to oligomerization [39]. The evaporation coefficient increase by one magnitude when the M increases beyond $500g/mol$, however this value of the molecular weight is a high value that does not represent the molecular weight of a freshly produced SOA. We also present the results of varying the gas diffusion coefficient on the evaporation coefficient (Figure 4.5). The evaporation coefficient decreases with increasing diffusion coefficient, however the effect is not pronounced and is constrained within the same order of magnitude. Therefore, the diffusion coefficient and molecular weight assumptions do not change the evaporation coefficient significantly.

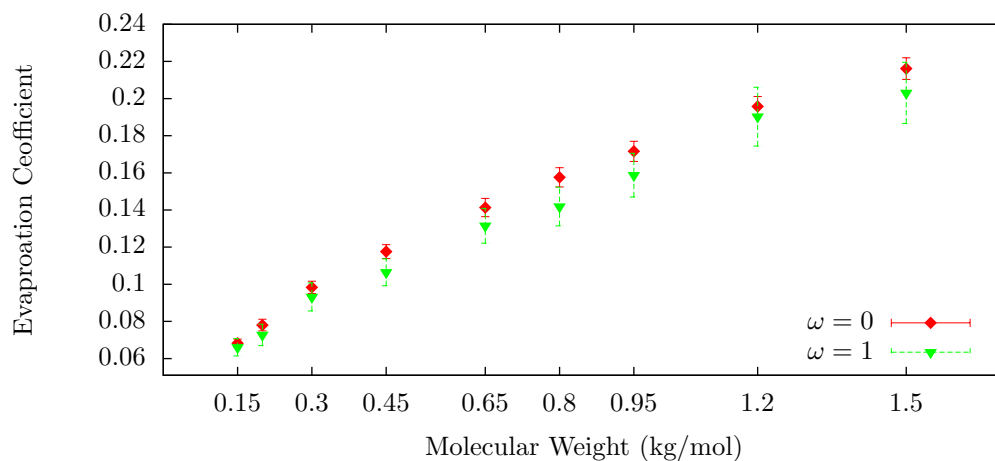


Figure 4.4: The variation of the evaporation coefficient as a function of molecular weights modelled using the results of experiment C.

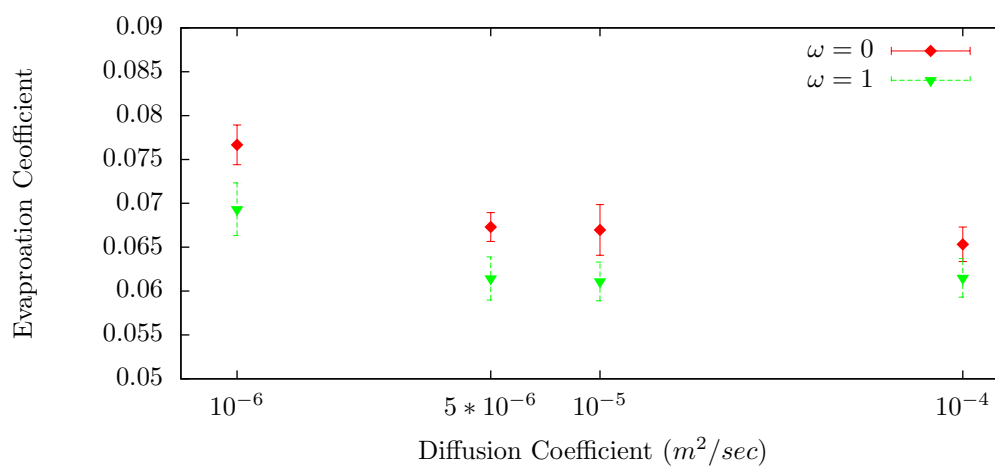


Figure 4.5: The variation of the evaporation coefficient as a function of gas diffusion coefficient modelled using the results of experiment C.

Chapter 5

Discussion

The aim of our experiments was to determine the evaporation coefficient without assuming the thermodynamic properties of the SOA used. From the equilibrium data and the evaporation coefficient we were able to demonstrate the ability of the system to reach equilibrium within an hour of perturbation.

5.1 SOA Volatility

We first compare the volatility of SOA produced in our PAM chamber from an anthropogenic source to others reported in literature. We are unable to provide an accurate measure of the saturation concentration because gas phase buildup commences during dilution while the evaporation model receives an initial gas phase concentration of 0 at the onset of decay after dilution. We however, provide a lower limit of the saturation concentration of anthropogenic SOA. The saturation concentrations of SOA measured in our experiment at 298K are listed in Table 5.1 along with the total organic concentration and the

organic aerosol concentration at equilibrium. We examine the volatilities of laboratory produced and ambient organic aerosols reported in literature. Since the total organic concentrations (C_{tot}) differ, mostly greater, from our considered cases we expect our results to have lower saturation concentrations [73]. Figure 5.1 is a scatter plot of the organic aerosol concentration (C_{OA}) versus the saturation concentration (C_g^*) from various publications [74, 75, 76, 24], each label data point exists on the line representing the combination between organic aerosol and gas concentration to add to the total organic concentration such that ($C_{tot} = C_{OA} + C_g^*$).

Table 5.1: Saturation Concentrations of SOA calculated from the four experiments at 298K

Experiment	C_{tot} ($\mu g/cm^3$)	C_{OA} ($\mu g/cm^3$)	C_g^* ($\mu g/cm^3$)
A	10.6	9.85	0.75
B	10.1	9.092	1.0078
C	10.1	9.29	0.81
D	9.63	8.31	1.31

Faulhaber *et al.* [74] produced SOA from the photochemical oxidation of pentadecane and diluted 10 folds from $150\mu g/m^3$ to $13.4\mu g/m^3$. Pentadecane SOA had $11.88\mu g/m^3$ in the condensed phase and $1.5\mu g/m^3$ in the gas phase at equilibrium. The volatility basis set used to calculate the results, based on yields adapted from Zeimman and Lim [77] was of oxidation products with volatility bins between $0.0001\mu g/m^3$ and $100\mu g/m^3$. SOA produced from the ozonolysis of α -pinene [24] indicates that most of organics material exist in the gas phase at equilibrium. For a total organic concentration of $10\mu g/m^3$ only $0.3\mu g/m^3$ existed in the condensed phase and $9.7\mu g/m^3$ existed in the gas

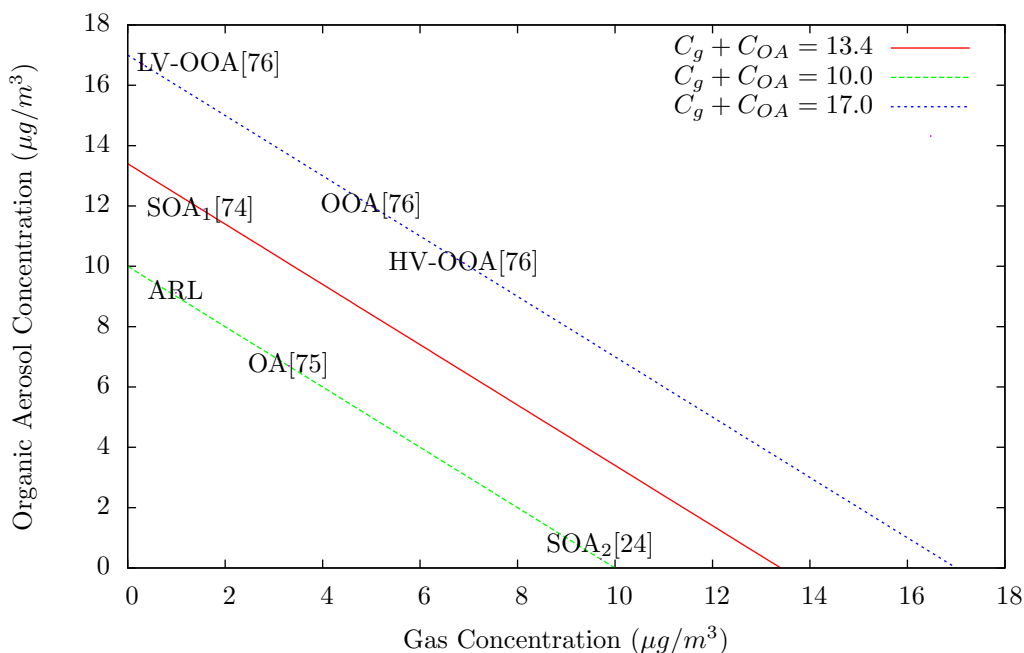


Figure 5.1: Saturation concentrations of organic aerosols cited in literature at 298K, ARL are the results from our experiments, LV-OOA is low volatility oxygenated organic aerosol, OOA is oxygenated organic aerosol, HV-OOA is high volatility oxygenated aerosol, OA is organic aerosol, SOA₁ produced from pentadecane, and SOA₂ from α -pinene.

phase. Cappa and Jimenez [76] determined the volatilities of different types of OA surrogates. SOA was represented by oxygenated organic aerosol (OOA), at a constant C_{OA} of $17\mu\text{g}/\text{m}^3$ and having an exponential relation between the total concentration and the saturation concentration at each bin. In the volatility basis set the largest considered saturation concentration bin(C^*) was $100\mu\text{g}/\text{m}^3$ and the least volatile was 10^{-5} with an evaporation coefficient of 1. For OOA, $12.4\mu\text{g}/\text{m}^3$ existed in the organic aerosol phase and $4.6\mu\text{g}/\text{m}^3$ in the gas phase. OOA had the lowest volatility between the considered surrogates of POA, biomass burning organic aerosol and anthropogenic combustion organic aerosol. OOA was further splitted into two subcomponents: (1) low volatility

OOA (LV-OOA) and (2) high volatility OOA (HV-OOA) where LV-OOA represent the volatility of the photochemically aged SOA, and the combination of concentrations is shown in Figure 5.1.

In order to compare with atmospherically relevant saturation concentrations, we show the results of Lee *et al.* [75] on the measurements of ambient OA. For a total concentration of $10\mu\text{g}/\text{m}^3$ $6.7\mu\text{g}/\text{m}^3$ existed in the particle phase and $3.3\mu\text{g}/\text{m}^3$ in the gas phase. The volatility reported in the study of Lee *et al.* [75] corresponds to aged organic aerosol accounting to both POA and SOA, while the results of Faulhaber *et al.* [74] and our results correspond to that of freshly produced SOA. This indicates that SOA produced in our PAM chamber from gasoline engine emissions is within the ranges of some of the reported volatilities of SOA in literature, especially freshly produced SOA.

5.2 Evaporation Coefficient

In our experiments we were able to demonstrate that engine exhaust SOA, at atmospherically relevant concentrations, reached equilibrium within an hour with an evaporation coefficient well constrained in the range of [0.01 0.1]. The present section delineates the consequences of our results.

Recently, there have been reports on the formation of amorphous solid SOA particles [34, 35] warranting the observations that SOA evaporation is limited by bulk mass transfer due to very low bulk diffusion coefficients [29]. Cappa and Wilson [76] reported that SOA evaporating in a TD did not reach equilibrium at the timescales available. SOA particles did not evaporate according to the volatilities of the compounds at which they were formed but layer by layer consistent with the behavior of a semi-solid particle. While the

amount of evidence of inhibited intrinsic mass transfer is increasing, our results of rapid equilibrium of SOA produced from a real anthropogenic SOA provide a counterstatement to those claims. Equilibrium is reached within an hour of dilution. In addition to that our surface to interface mass transfer model closely predicts the evaporation results from our experiments.

Contrary to the studies aiming at calculating equilibrium times, Vaden *et al.* [29] studied the evaporation rates of SOA. Since the approach relies on inciting evaporation by adding activated carbon to adsorb vapor in the chamber, evaporation rates were modeled using mass transfer equations at the surface of the particle. They calculated the saturation concentration of the SOA by using the results of the seven-product volatility basis set of α -pinene oxidized SOA under low NO_x and dark ozonolysis [24]. The observed slow evaporation rates were attributed to the intra-particle mass transfer resistance due to the amorphous state of the SOA particles; the evaporation rates were consistent with a very small evaporation coefficient less than 0.05. To demonstrate the importance of calculating the saturation concentration of the particles involved in a certain experiment, we calculated the evaporation coefficient corresponding to the evaporation of our particles before approaching equilibrium at different saturation concentrations (Figure 5.2).

As can be seen in the Figure 5.2 the model produces a fit at any saturation concentration. We have chosen the range of saturation concentrations to cover the values that will cause an order of magnitude decrease in the evaporation coefficient. While $C_{sat} = 0.87\mu\text{gm}^{-3}$ is the saturation concentration we calculated for our SOA particles at equilibrium, whenever the SOA particles are assumed to be more volatile than they are, a lower evaporation coefficient will be calculated than the actual value. In the case of the reported amorphous

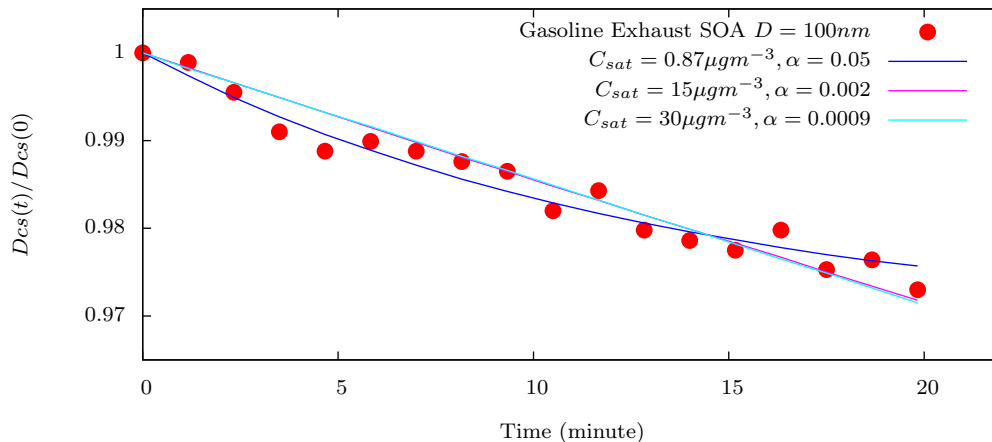


Figure 5.2: Model fit results of SOA particle evaporation before approaching equilibrium according to different values of saturation concentrations.

solid particle in the Vaden *et al.* approach, SOA will have a lower saturation concentration [72] than the ones parametrized using the absorptive partitioning theory, especially considering the long experimental time and the effects of aging. Therefore producing a fit to their experimental result is possible when the correct physical parameters are used.

Furthermore, other approaches have been observing slow evaporation rates of SOA particles due to the ongoing polymerization reactions, oligomerization, in the condensed phase beyond the irradiation exposure. Oligomerization leads to the production of high molecular weight and low volatility compounds [37, 39, 78]. In a similar experimental approach to ours of the isothermal dilution of freshly produced α -pinene SOA in a smog chamber [44], oligomerization was reported to be responsible to the recorded sluggish evaporation rates and to the evaporation coefficient range of [0.001 0.01]. However, SOA particles in our experiment reached equilibrium in 1 hour and we did not observe any distinct evaporation phases as reported by Donahue and Trump [27].

The presence of oligomers in freshly produced SOA cannot be corroborated by the present literature on oligomer formation because the oligomerization is being evaluated after time periods more than four times greater than the entire experiment period [39, 37]. Thus, evidence that freshly-produced SOA particles form oligomers is not yet founded.

More recently, Saleh *et al.* [52] published results of freshly-produced SOA particles reaching equilibrium within minutes of subjecting particles to a temperature step change. They then calculated the evaporation coefficient to be in the range [0.1 1], similar to the coefficient of a single component dicarboxylic acid that does not have intra-particle mass transfer resistance. The difference between measurements of the evaporation rates, equilibration times and evaporation coefficients recorded maybe due to the considered timescales of experiments, if oligomerization was recognized as the cause of hindrance of evaporation [79]. The SOA produced by Vaden *et al.* and that by Grieshop [44] can be aged under the timescales of the experiment and both studies use saturation concentrations that are reported for freshly produced α -pinene yields. However, both studies concede to the effects of aging on the response of particles. Consequently, with the current state of research we cannot yet distinguish between the evaporation coefficient calculated for aged or freshly produced aerosol. Results computed in our experiments using SOA produced from anthropogenic SOA show that mass transfer is not the rate limiting step in evaporation.

Chapter 6

Conclusion

In our approach of isothermal dilution to measure the evaporation kinetics of SOA in atmospherically relevant conditions we calculated the evaporation coefficient to be 0.063 and the equilibration times were in the range of an hour for the concentrations considered in the experiments.

- Rate loss to the walls is a diameter-dependent process. Smaller particles (<200nm) deposit on surfaces, due to diffusion into the material, more than larger particles (>200nm).
- The evaporation coefficient is weakly dependent on the wall-suspension partitioning coefficient (ω).
- In contrast to some recent studies on biogenic SOA, we found that SOA reached equilibrium within an hour of dilution. Observations were consistent with absorptive partitioning phenomena and did not require resort to more complex models such as oligomer dissociation.
- More work is needed to evaluate the effect of aging and bulk to surface diffusion hindrance to be able to provide an argument inclusive of re-

sults not just based on freshly produced SOA but on particles that were present for longer times before being transported and deposited on surfaces.

Appendix A

Abbreviations

SOA	Secondary Organic Aerosol
POA	Primary Organic Aerosol
PAM	Potential Aerosol Mass
DMA	Differential Mobility Analyzer
CPC	Condensation Particle Counter
SMPS	Scanning Mobility Particle Sizer
PFA	Perfluoroalkoxy Alkane
TD	Thermodenuder
OOA	Oxygenated Organic Aerosols
HV-OOA	High volatility Oxygenated Organic Aerosols
LV-OOA	Low volatility Oxygenated Organic Aerosols
ARL	Aerosol Research Lab
SR	Saturation Ratio
J_A	Molar Flux
C_{sat}	Saturation Concentration
C_{OA}	Organic Aerosol Concentration

C_g	Gas Phase Concentration
$D_{A,B}$	Diffusion Coefficient
r	Radius
M	Molecular Weight
k	Boltzmann's Constant
T	Temperature
K	Kelvin Correction Factor
σ	Surface Tension
N_0	Avogadro's Number
d_p	Particle Diameter
ρ	Density
λ	Mean Free Path
Kn	Knudsen Number
α	Evaporation Coefficient
C_m	Fuchs Sutugin Correction Factor
β	Wall loss rate
ω	Wall-Suspension Partitioning Factor
N_{sus}	Number Concentration of Suspended Particles
N_{deps}	Number Concentration of Deposited Particles
N_{total}	Total Number Concentration
CS	Condensation Sink
d_{cs}	Condensation Sink Diameter
a	Growth Factor

Bibliography

- [1] D. W. Dockery, C. A. Pope, X. Xu, J. D. Spengler, J. H. Ware, M. E. Fay, B. G. Ferris Jr, and F. E. Speizer, “An association between air pollution and mortality in six us cities,” *New England journal of medicine*, vol. 329, no. 24, pp. 1753–1759, 1993.

- [2] U. S. E. P. Agency, “Particulate matter (pm),” 2013.

- [3] D. Murphy, D. Cziczo, K. Froyd, P. Hudson, B. Matthew, A. Middlebrook, R. E. Peltier, A. Sullivan, D. Thomson, and R. Weber, “Single-particle mass spectrometry of tropospheric aerosol particles,” *Journal of Geophysical Research: Atmospheres (1984–2012)*, vol. 111, no. D23, 2006.

- [4] C. N. Cruz and S. N. Pandis, “A study of the ability of pure secondary organic aerosol to act as cloud condensation nuclei,” *Atmospheric Environment*, vol. 31, no. 15, pp. 2205–2214, 1997.

- [5] M. Kanakidou, J. Seinfeld, S. Pandis, I. Barnes, F. Dentener, M. Facchini, R. V. Dingenen, B. Ervens, A. Nenes, C. Nielsen, *et al.*, “Organic aerosol and global climate modelling: a review,” *Atmospheric Chemistry and Physics*, vol. 5, no. 4, pp. 1053–1123, 2005.

- [6] J. Jimenez, M. Canagaratna, N. Donahue, A. Prevot, Q. Zhang, J. Kroll, P. DeCarlo, J. Allan, H. Coe, N. Ng, *et al.*, “Evolution of organic aerosols in the atmosphere,” *Science*, vol. 326, no. 5959, pp. 1525–1529, 2009.
- [7] A. Ortega, D. Day, M. Cubison, W. Brune, D. Bon, J. de Gouw, and J. Jimenez, “Secondary organic aerosol formation and primary organic aerosol oxidation from biomass-burning smoke in a flow reactor during flame-3,” *Atmospheric Chemistry and Physics*, vol. 13, no. 22, pp. 11551–11571, 2013.
- [8] J. De Gouw, A. Middlebrook, C. Warneke, P. Goldan, W. Kuster, J. Roberts, F. Fehsenfeld, D. Worsnop, M. Canagaratna, A. Pszenny, *et al.*, “Budget of organic carbon in a polluted atmosphere: Results from the new england air quality study in 2002,” *Journal of Geophysical Research: Atmospheres (1984–2012)*, vol. 110, no. D16, 2005.
- [9] R. Volkamer, J. L. Jimenez, F. San Martini, K. Dzepina, Q. Zhang, D. Salcedo, L. T. Molina, D. R. Worsnop, and M. J. Molina, “Secondary organic aerosol formation from anthropogenic air pollution: Rapid and higher than expected,” *Geophysical Research Letters*, vol. 33, no. 17, 2006.
- [10] J. F. Pankow, “An absorption model of the gas/aerosol partitioning involved in the formation of secondary organic aerosol,” *Atmospheric Environment*, vol. 28, no. 2, pp. 189–193, 1994.
- [11] J. F. Pankow, “An absorption model of gas/particle partitioning of organic compounds in the atmosphere,” *Atmospheric Environment*, vol. 28, no. 2, pp. 185–188, 1994.

- [12] A. Chan, J. Kroll, N. Ng, and J. Seinfeld, “Kinetic modeling of secondary organic aerosol formation: effects of particle-and gas-phase reactions of semivolatile products,” *Atmospheric Chemistry and Physics*, vol. 7, no. 15, pp. 4135–4147, 2007.
- [13] P. E. Sheehan and F. M. Bowman, “Estimated effects of temperature on secondary organic aerosol concentrations,” *Environmental science & technology*, vol. 35, no. 11, pp. 2129–2135, 2001.
- [14] R. Lohmann and G. Lammel, “Adsorptive and absorptive contributions to the gas-particle partitioning of polycyclic aromatic hydrocarbons: state of knowledge and recommended parametrization for modeling,” *Environmental science & technology*, vol. 38, no. 14, pp. 3793–3803, 2004.
- [15] E. M. Lipsky and A. L. Robinson, “Effects of dilution on fine particle mass and partitioning of semivolatile organics in diesel exhaust and wood smoke,” *Environmental science & technology*, vol. 40, no. 1, pp. 155–162, 2006.
- [16] S. Lee, M. Jang, and R. M. Kamens, “Soa formation from the photooxidation of α -pinene in the presence of freshly emitted diesel soot exhaust,” *Atmospheric Environment*, vol. 38, no. 16, pp. 2597–2605, 2004.
- [17] D. R. Cocker III, S. L. Clegg, R. C. Flagan, and J. H. Seinfeld, “The effect of water on gas-particle partitioning of secondary organic aerosol. part I: α -pinene/ozone system,” *Atmospheric Environment*, vol. 35, no. 35, pp. 6049–6072, 2001.
- [18] R. J. Griffin, D. R. Cocker, R. C. Flagan, and J. H. Seinfeld, “Organic aerosol formation from the oxidation of biogenic hydrocarbons,” *Jour-*

nal of Geophysical Research: Atmospheres (1984–2012), vol. 104, no. D3, pp. 3555–3567, 1999.

- [19] R. Volkamer, P. Ziemann, and M. Molina, “Secondary organic aerosol formation from acetylene (c 2 h 2): seed effect on soa yields due to organic photochemistry in the aerosol aqueous phase,” *Atmospheric Chemistry and Physics*, vol. 9, no. 6, pp. 1907–1928, 2009.
- [20] S. N. Pandis, R. A. Harley, G. R. Cass, and J. H. Seinfeld, “Secondary organic aerosol formation and transport,” *Atmospheric Environment. Part A. General Topics*, vol. 26, no. 13, pp. 2269 – 2282, 1992.
- [21] J. R. Odum, T. Hoffmann, F. Bowman, D. Collins, R. C. Flagan, and J. H. Seinfeld, “Gas/particle partitioning and secondary organic aerosol yields,” *Environmental Science & Technology*, vol. 30, no. 8, pp. 2580–2585, 1996.
- [22] C. Liang, J. F. Pankow, J. R. Odum, and J. H. Seinfeld, “Gas/particle partitioning of semivolatile organic compounds to model inorganic, organic, and ambient smog aerosols,” *Environmental science & technology*, vol. 31, no. 11, pp. 3086–3092, 1997.
- [23] K. M. Henry, T. Lohaus, and N. M. Donahue, “Organic aerosol yields from α -pinene oxidation: bridging the gap between first-generation yields and aging chemistry,” *Environmental science & technology*, vol. 46, no. 22, pp. 12347–12354, 2012.
- [24] R. Pathak, A. Presto, T. Lane, C. Stanier, N. Donahue, and S. Pandis, “Ozonolysis of α -pinene: parameterization of secondary organic

- aerosol mass fraction,” *Atmospheric Chemistry and Physics*, vol. 7, no. 14, pp. 3811–3821, 2007.
- [25] T. Hoffmann, J. R. Odum, F. Bowman, D. Collins, D. Klockow, R. C. Flanagan, and J. H. Seinfeld, “Formation of organic aerosols from the oxidation of biogenic hydrocarbons,” *Journal of Atmospheric Chemistry*, vol. 26, no. 2, pp. 189–222, 1997.
- [26] N. Donahue, A. Robinson, C. Stanier, and S. Pandis, “Coupled partitioning, dilution, and chemical aging of semivolatile organics,” *Environmental Science & Technology*, vol. 40, no. 8, pp. 2635–2643, 2006.
- [27] E. Trump and N. Donahue, “Oligomer formation within secondary organic aerosols: equilibrium and dynamic considerations,” *Atmospheric Chemistry and Physics*, vol. 14, no. 7, pp. 3691–3701, 2014.
- [28] A. A. Presto, K. E. Huff Hartz, and N. M. Donahue, “Secondary organic aerosol production from terpene ozonolysis. 2. effect of no x concentration,” *Environmental science & technology*, vol. 39, no. 18, pp. 7046–7054, 2005.
- [29] T. D. Vaden, D. Imre, J. Beránek, M. Shrivastava, and A. Zelenyuk, “Evaporation kinetics and phase of laboratory and ambient secondary organic aerosol,” *Proceedings of the National Academy of Sciences*, vol. 108, no. 6, pp. 2190–2195, 2011.
- [30] C. D. Cappa and K. R. Wilson, “Evolution of organic aerosol mass spectra upon heating: implications for oa phase and partitioning behavior,” *Atmospheric Chemistry and Physics*, vol. 11, no. 5, pp. 1895–1911, 2011.

- [31] K. Dzepina, R. M. Volkamer, S. Madronich, P. Tulet, I. M. Ulbrich, Q. Zhang, C. D. Cappa, P. J. Ziemann, and J. L. Jimenez, “Evaluation of recently-proposed secondary organic aerosol models for a case study in Mexico City,” *Atmospheric Chemistry and Physics*, vol. 9, no. 15, pp. 5681–5709, 2009.
- [32] C. O. Stanier, R. K. Pathak, and S. N. Pandis, “Measurements of the volatility of aerosols from α -pinene ozonolysis,” *Environmental Science & Technology*, vol. 41, no. 8, pp. 2756–2763, 2007.
- [33] A. Virtanen, J. Joutsensaari, T. Koop, J. Kannosto, P. Yli-Pirilä, J. Leskinen, J. M. Mäkelä, J. K. Holopainen, U. Pöschl, M. Kulmala, *et al.*, “An amorphous solid state of biogenic secondary organic aerosol particles,” *Nature*, vol. 467, no. 7317, pp. 824–827, 2010.
- [34] B. Zobrist, C. Marcolli, D. Pedernera, and T. Koop, “Do atmospheric aerosols form glasses?,” *Atmospheric Chemistry and Physics*, vol. 8, no. 17, pp. 5221–5244, 2008.
- [35] E. Mikhailov, S. Vlasenko, S. Martin, T. Koop, and U. Pöschl, “Amorphous and crystalline aerosol particles interacting with water vapor: conceptual framework and experimental evidence for restructuring, phase transitions and kinetic limitations,” *Atmospheric Chemistry and Physics*, vol. 9, no. 24, pp. 9491–9522, 2009.
- [36] U. Baltensperger, M. Kalberer, J. Dommen, D. Paulsen, M. Alfarra, H. Coe, R. Fisseha, A. Gascho, M. Gysel, S. Nyeki, *et al.*, “Secondary organic aerosols from anthropogenic and biogenic precursors,” *Faraday Discussions*, vol. 130, pp. 265–278, 2005.

- [37] S. Gao, M. Keywood, N. L. Ng, J. Surratt, V. Varutbangkul, R. Bahreini, R. C. Flagan, and J. H. Seinfeld, “Low-molecular-weight and oligomeric components in secondary organic aerosol from the ozonolysis of cycloalkenes and α -pinene,” *The Journal of Physical Chemistry A*, vol. 108, no. 46, pp. 10147–10164, 2004.
- [38] K. J. Heaton, M. A. Dreyfus, S. Wang, and M. V. Johnston, “Oligomers in the early stage of biogenic secondary organic aerosol formation and growth,” *Environmental Science & Technology*, vol. 41, no. 17, pp. 6129–6136, 2007. PMID: 17937292.
- [39] M. R. Alfarra, D. Paulsen, M. Gysel, A. A. Garforth, J. Dommen, A. S. Prévôt, D. R. Worsnop, U. Baltensperger, and H. Coe, “A mass spectrometric study of secondary organic aerosols formed from the photooxidation of anthropogenic and biogenic precursors in a reaction chamber,” *Atmospheric Chemistry and Physics*, vol. 6, no. 12, pp. 5279–5293, 2006.
- [40] V. Perraud, E. A. Bruns, M. J. Ezell, S. N. Johnson, Y. Yu, M. L. Alexander, A. Zelenyuk, D. Imre, W. L. Chang, D. Dabdub, *et al.*, “Nonequilibrium atmospheric secondary organic aerosol formation and growth,” *Proceedings of the National Academy of Sciences*, vol. 109, no. 8, pp. 2836–2841, 2012.
- [41] L. Hildebrandt, K. M. Henry, J. H. Kroll, D. R. Worsnop, S. N. Pandis, and N. M. Donahue, “Evaluating the mixing of organic aerosol components using high-resolution aerosol mass spectrometry,” *Environmental science & technology*, vol. 45, no. 15, pp. 6329–6335, 2011.

- [42] E. S. Robinson, R. Saleh, and N. M. Donahue, “Organic aerosol mixing observed by single-particle mass spectrometry,” *The Journal of Physical Chemistry A*, vol. 117, no. 51, pp. 13935–13945, 2013.
- [43] C. L. Loza, M. M. Coggon, T. B. Nguyen, A. Zuend, R. C. Flagan, and J. H. Seinfeld, “On the mixing and evaporation of secondary organic aerosol components,” *Environmental science & technology*, vol. 47, no. 12, pp. 6173–6180, 2013.
- [44] A. P. Grieshop, N. M. Donahue, and A. L. Robinson, “Is the gas-particle partitioning in alpha-pinene secondary organic aerosol reversible?,” *Geophysical Research Letters*, vol. 34, no. 14, 2007.
- [45] R. Saleh, N. M. Donahue, and A. L. Robinson, “Time scales for gas-particle partitioning equilibration of secondary organic aerosol formed from alpha-pinene ozonolysis,” *Environmental science & technology*, vol. 47, no. 11, pp. 5588–5594, 2013.
- [46] E. J. Davis and G. Schweiger, *The airborne microparticle: its physics, chemistry, optics, and transport phenomena*. Springer, 2002.
- [47] J. H. Seinfeld and S. N. Pandis, *Atmospheric chemistry and physics: from air pollution to climate change*. John Wiley & Sons, 2012.
- [48] N. Fuks and A. Sutugin, “Highly dispersed aerosols (vysokodispersne aerosoli),” tech. rep., DTIC Document, 1971.
- [49] J. Brock, “Highly nonequilibrium evaporation of moving particles in the transition region of knudsen number,” *Journal of Colloid and Interface Science*, vol. 24, no. 3, pp. 344–351, 1967.

- [50] J. C. Maxwell, “V. illustrations of the dynamical theory of gases.part i. on the motions and collisions of perfectly elastic spheres,” *The London, Edinburgh, and Dublin Philosophical Magazine and Journal of Science*, vol. 19, no. 124, pp. 19–32, 1860.
- [51] P. McMurry and D. Rader, “Aerosol wall losses in electrically charged chambers,” *Aerosol Science and Technology*, vol. 4, no. 3, pp. 249–268, 1985.
- [52] R. Saleh, A. Shihadeh, and A. Khlystov, “On transport phenomena and equilibration time scales in thermodenuders,” *Atmospheric Measurement Techniques*, vol. 4, no. 3, pp. 571–581, 2011.
- [53] R. Saleh, A. Khlystov, and A. Shihadeh, “Determination of evaporation coefficients of ambient and laboratory-generated semivolatile organic aerosols from phase equilibration kinetics in a thermodenuder,” *Aerosol Science and Technology*, vol. 46, no. 1, pp. 22–30, 2012.
- [54] G. Mann, K. Carslaw, D. Ridley, D. Spracklen, K. Pringle, J. Merikanto, H. Korhonen, J. Schwarz, L. Lee, P. Manktelow, *et al.*, “Intercomparison of modal and sectional aerosol microphysics representations within the same 3-d global chemical transport model,” *Atmospheric Chemistry and Physics*, vol. 12, no. 10, pp. 4449–4476, 2012.
- [55] K. E. Lehtinen, H. Korhonen, M. Maso, and M. Kulmala, “On the concept of condensation sink diameter,” *Boreal environment research*, vol. 8, no. 4, pp. 405–412, 2003.
- [56] W. P. Carter, D. R. Cocker III, D. R. Fitz, I. L. Malkina, K. Bumiller, C. G. Sauer, J. T. Pisano, C. Bufalino, and C. Song, “A new environ-

- mental chamber for evaluation of gas-phase chemical mechanisms and secondary aerosol formation,” *Atmospheric Environment*, vol. 39, no. 40, pp. 7768–7788, 2005.
- [57] M. Kalberer, M. Sax, and V. Samburova, “Molecular size evolution of oligomers in organic aerosols collected in urban atmospheres and generated in a smog chamber,” *Environmental science & technology*, vol. 40, no. 19, pp. 5917–5922, 2006.
- [58] H. Takekawa, H. Minoura, A. Yasuda, *et al.*, “Construction and characterization of an atmospheric simulation smog chamber,” *Advances in Atmospheric Sciences*, vol. 24, no. 2, pp. 250–258, 2007.
- [59] E. Nordin, A. Eriksson, P. Roldin, P. Nilsson, J. Carlsson, M. Kajos, H. Hellén, C. Wittbom, J. Rissler, J. Löndahl, *et al.*, “Secondary organic aerosol formation from idling gasoline passenger vehicle emissions investigated in a smog chamber,” *Atmospheric Chemistry and Physics*, vol. 13, no. 12, pp. 6101–6116, 2013.
- [60] E. Kang, M. Root, D. Toohey, and W. Brune, “Introducing the concept of potential aerosol mass (pam),” *Atmospheric Chemistry and Physics*, vol. 7, no. 22, pp. 5727–5744, 2007.
- [61] M. Lindskog and E. Nordin, “Ageing of diesel aerosols: Design and implementation of ateflon simulation chamber,” Master’s thesis, Lund University, May 2009.
- [62] R. Saleh, A. Shihadeh, and A. Khlystov, “Determination of evaporation coefficients of semi-volatile organic aerosols using an integrated volumetan-

- dem differential mobility analysis (iv-tdma) method,” *Journal of Aerosol Science*, vol. 40, no. 12, pp. 1019–1029, 2009.
- [63] R. Saleh, A. Khlystov, and A. Shihadeh, “Determination of evaporation coefficients of ambient and laboratory-generated semivolatile organic aerosols from phase equilibration kinetics in a thermodenuder,” *Aerosol Science and Technology*, vol. 46, no. 1, pp. 22–30, 2012.
- [64] P. D. Kinney and D. Y. Pui, “Use of the electrostatic classification method to 0.1 μm srm particles—a feasibility study,” *Journal of Research of the National Institute of Standards and Technology*, vol. 96, no. 2, 1991.
- [65] C. Loza, P. Chhabra, L. Yee, J. Craven, R. Flagan, and J. Seinfeld, “Chemical aging of m-xylene secondary organic aerosol: laboratory chamber study,” *Atmospheric Chemistry and Physics*, vol. 12, no. 1, pp. 151–167, 2012.
- [66] J. G. Crump, R. C. Flagan, and J. H. Seinfeld, “Particle wall loss rates in vessels,” *Aerosol Science and Technology*, vol. 2, no. 3, pp. 303–309, 1982.
- [67] J. Pierce, G. Engelhart, L. Hildebrandt, E. Weitkamp, R. Pathak, N. Donahue, A. Robinson, P. Adams, and S. Pandis, “Constraining particle evolution from wall losses, coagulation, and condensation-evaporation in smog-chamber experiments: optimal estimation based on size distribution measurements,” *Aerosol Science and Technology*, vol. 42, no. 12, pp. 1001–1015, 2008.
- [68] R. S. Figliola and D. E. Beasley, “Theory and design for mechanical measurements,” *Measurement Science and Technology*, vol. 12, no. 10, p. 1743, 2001.

- [69] A. S. Wexler and J. H. Seinfeld, “The distribution of ammonium salts among a size and composition dispersed aerosol,” *Atmospheric Environment. Part A. General Topics*, vol. 24, no. 5, pp. 1231–1246, 1990.
- [70] R. Saleh, A. Khlystov, and A. Shihadeh, “Effect of aerosol generation method on measured saturation pressure and enthalpy of vaporization for dicarboxylic acid aerosols,” *Aerosol Science and Technology*, vol. 44, no. 4, pp. 302–307, 2010.
- [71] E. A. Weitkamp, A. M. Sage, J. R. Pierce, N. M. Donahue, and A. L. Robinson, “Organic aerosol formation from photochemical oxidation of diesel exhaust in a smog chamber,” *Environmental science & technology*, vol. 41, no. 20, pp. 6969–6975, 2007.
- [72] M. Shiraiwa and J. H. Seinfeld, “Equilibration timescale of atmospheric secondary organic aerosol partitioning,” *Geophysical Research Letters*, vol. 39, no. 24, 2012.
- [73] J. Zhang, K. E. Huff Hartz, S. N. Pandis, and N. M. Donahue, “Secondary organic aerosol formation from limonene ozonolysis: Homogeneous and heterogeneous influences as a function of no_x ,” *The Journal of Physical Chemistry A*, vol. 110, no. 38, pp. 11053–11063, 2006.
- [74] A. Faulhaber, B. Thomas, J. Jimenez, J. Jayne, D. Worsnop, and P. Ziemann, “Characterization of a thermodenuder-particle beam mass spectrometer system for the study of organic aerosol volatility and composition,” *Atmospheric Measurement Techniques*, vol. 2, no. 1, pp. 15–31, 2009.

- [75] B. Lee, E. Kostenidou, L. Hildebrandt, I. Riipinen, G. Engelhart, C. Mohr, P. DeCarlo, N. Mihalopoulos, A. Prevot, U. Baltensperger, *et al.*, “Measurement of the ambient organic aerosol volatility distribution: application during the finokalia aerosol measurement experiment (fame-2008),” *Atmospheric Chemistry and Physics*, vol. 10, no. 24, pp. 12149–12160, 2010.
- [76] C. Cappa and J. Jimenez, “Quantitative estimates of the volatility of ambient organic aerosol,” *Atmospheric Chemistry and Physics*, vol. 10, no. 12, pp. 5409–5424, 2010.
- [77] Y. B. Lim and P. J. Ziemann, “Products and mechanism of secondary organic aerosol formation from reactions of n-alkanes with oh radicals in the presence of no x,” *Environmental science & technology*, vol. 39, no. 23, pp. 9229–9236, 2005.
- [78] M. Kalberer, D. Paulsen, M. Sax, M. Steinbacher, J. Dommen, A. Prevot, R. Fisseha, E. Weingartner, V. Frankevich, R. Zenobi, *et al.*, “Identification of polymers as major components of atmospheric organic aerosols,” *Science*, vol. 303, no. 5664, pp. 1659–1662, 2004.
- [79] P. Roldin, A. Eriksson, E. Nordin, E. Hermansson, D. Mogensen, A. Rusanen, M. Boy, E. Swietlicki, B. Svenningsson, A. Zelenyuk, *et al.*, “Modelling non-equilibrium secondary organic aerosol formation and evaporation with the aerosol dynamics, gas-and particle-phase chemistry kinetic multi-layer model adcham,” *Atmospheric Chemistry and Physics Discussions*, vol. 14, no. 1, pp. 769–869, 2014.